DISSERTATION

Role of histone variant H3.3 in neurogenesis and gliomagenesis

Pablo Bellvís Zambrano

2017

Dissertation

submitted to the

Combined Faculties for the Natural Sciences and for Mathematics

of the Ruperto-Carola University of Heidelberg, Germany

for the degree of

Doctor of Natural Sciences

presented by

Master of Science Pablo Bellvís Zambrano

born in: Sevilla, Spain

Oral-examination: 6th July, 2017

Role of histone variant H3.3 in neurogenesis and gliomagenesis

Referees: Prof. Dr. Ana Martin-Villalba

Dr. Haikun Liu

Acknowledgements

I would like to start by thanking my supervisor Hai-Kun for giving me the opportunity to work in this project for my PhD. I would also like to thank Weijun for teaching me many of the techniques that I used in the lab, as well as for his help developing my critical thinking to apply when designing experiments.

I would also like to thank the DKFZ for providing me with a great environment to do science. I especially would like to thank Frank and Ulrich, from the Transgenic Service for their advice and expertise in developing the transgenic mice. I am thankful to my TAC members Prof. Dr. Michael Boutros and Prof. Dr. Christel Herold-Mende for their guidance and feedback during my PhD.

I would like to thank every former and current member of the A240 for sharing this time with me. I would like to especially mention some members that helped me considerably during this period both scientifically and personally. My gratitude goes to Olga, for her logistic support and friendship, I really really thank you. To Gözde and Malin, for sharing so many evenings with me at work and keeping up my motivation with our talks. To my lab buddies Daniela and Patricia, for providing manly conversations and humor when necessary. To Azer, for connecting me with the younger generation, for our enjoyable discussions, our OCD and all what we shared outside the lab. You know what we say Azer.

Last but not least, I would like to thank my friends and family for the constant support. I would like to thank Isa for so many things that would not fit in a page. There is a saying that states that behind every great man is a great woman, I achieved the difficult part finding myself a great woman. Now I just need to become a great man. Finally, my greatest gratitude to my little Pablo, you have been a constant source of happiness during your first year. I thank you for cheering me up every morning when you wake up and every evening when you see me arriving, I love you.

Table of contents

Abbreviations

AEBP2 Adipocyte Enhancer-Binding Protein 2

AKT Protein Kinase B

ASF1 antisilencing function protein 1

ASLV Avian sarcoma-leukosis Virus

CAF-1 chromatin assembly factor-1

CCND1/2/3 Cyclin D1/2/3

CDK4/6 Cyclin-dependent kinase 4/6

CDKN2A cyclin-dependent kinase inhibitor 2A

CENP-A Centromeric protein A

CNS Central nervous system

DAXX/ATRX death-domain-associated protein/α-thalassemia and mental retardation syndrome X-linked protein

DIPG Diffuse intrinsic pontine glioma

DNA Deoxy-ribonucleotide acid

DSC DNA synthesis-coupled

DSI DNA synthesis-independent

E9.5 Embryonic day 9.5

EED Embryonic ectoderm development

ES embryonic stem

EZH1/2 Enhancer of zeste 1/2

FOXG1 forkhead box G1

G34R/V glycine 34 to arginine/valine mutation

GABA Gamma aminobutyric acid

GBM Glioblastoma multiforme

H3K27AC Histone 3 lysine 27 acetylation

H3K27me2 Histone 3 lysine 27 dimethylation

H3K27me3 Histone 3 lysine 27 trimethylation

H3K36me2 Histone 3 lysine 36 dimethylation

H3K36me3 Histone 3 lysine 36 trimethylation

H3K4me3 Histone 3 lysine 4 trimethylation

H4K16Ac Histone 4 Lysine 16 Acetylation

HIRA histone regulator A

IGF1R insulin-like growth factor 1 receptor

JARID2 Jumonji And AT-Rich Interaction Domain Containing 2

Jmj Jumonji

K27M Lysine 27 to methionine mutation

K27me3 Lysine 27 trimethylation

LTR long terminal repeats

MEF Mouse Embryonic Fibroblast

MET mesenchymal epithelial transition factor

MRI Magnetic resonance imaging

mRNA messenger ribonucleotide acid

NPC Neuronal precursor cell

OLIG2 Oligodendrocyte transcription factor

PCL Polycomb-like

PDGF platelet-derived growth factor

PDGFRA platelet-derived growth factor receptor-α

PHD plant homeodomain

PI3K Phosphoinositide 3-kinase

PRC2 Polycomb repressive complex 2

PTEN Phosphatase and tensin homolog

PTM Post-transcriptional modification

RB Retinoblastoma

RbAp46/48 Retinoblastoma-associated proteins 46/48

RCAS Replication-Competent Avian sarcoma-leukosis Virus with Splice acceptor

RNA Ribonucleotide acid

RTK receptor tyrosine kinase

SUZ12 Supressor of zeste 12

SVM Serine, Valine and Methionine

SVZ subventricular zone

UV Ultraviolet

TSS Transcriptional start site

WHO World Health Organization

Summary

Glioblastoma multiforme (GBM) (WHO classification IV) is the most common primary malignant brain tumor with a poor prognosis in both adults and children. In the last years several studies have shown that 44% of glioblastoma multiforme tumors are characterized by the same histone mutations manifested in the histone variant H3.3. These studies strongly implicate the K27M amino acid substitution in H3.3 in the pathogenesis of diffuse intrinsic pontine glioma (DIPG). Also, H3.3 has been recently linked to multiple processes in the brain like neuronal specialization, synapses, cognition and contextual fear memory.

In this study, two important tools were generated to investigate the role of H3.3 in the brain. Firstly, making use of the RCAS/TVA system, we established a DIPG mouse model overexpressing constitutively active AKT, PDGFB, Luciferase and floxed H3.3K27M in Nestin expressing cells in the brain. This model resembles High Grade Gliomas (HGGs) in histology and shows a key feature observed in the human DIPG tumors that is the H3K27me3 loss. In combination with Bioluminescence Imaging (BLI), the model enables monitoring of tumor growth. The model allowed for H3K27me3 recovery after deletion of H3.3K27M.

Secondly, we successfully established an inducible RFP-tagged H3f3b-overexpressing mouse line. By modifying a Bacterial Artificial Chromosome (BAC) carrying the H3f3b gene, the fusion protein H3f3b-RFP-ERT2 was overexpressed. This construct allows for histone tracing in living behaving animals.

Zusammenfassung

Glioblastoma multiforme (GBM) (WHO Klasse IV) ist der häufigste primäre bösartige Gehirntumor, mit einer schlechten Prognose sowohl für Erwachsene wie auch für Kinder. Verschiedene Studien der letzten Jahre haben gezeigt, dass 44% der GBM Tumore durch bestimmte Mutationen in der Histonvariante H3.3 charakterisiert sind. Diese Studien deuten stark darauf hin, dass im diffus intrinsisichen Ponsgliom (DIPG) ein K27M Aminosäurenaustausch in H3.3 stattfand. Des Weiteren wurde H3.3 mit vielen anderen Prozessen in Verbindung gebracht, wie neuronale Spezialisierung im Gehirn, Synapsen, kognitives und kontextuelles Angstgedächtnis.

In der hier vorliegenden Arbeit wurden zwei wichtige Methoden entwickelt um die Rolle von H3.3 im Gehirn zu analysieren. Als erstes wurde das RCAS/TVA System benutzt um ein Mausmodel für DIPG, durch Überexpressison von konstitutiv aktivem AKT, PDGFRB, Luciferase und gefloxtem H3.3K27M in Nestin exprimierenden Zellen im Mausgehirn, entwickelt. Diese Modell hat eine ähnliche Histologie wie hochgradige Gliomas (HGGs) und zeigt ein Kennzeichen welches in humanen DIPG Tumoren beobachtet wurde, den Verlust von H3K27me3. In Verbindung mit bioluniniszenter Bildgebung kann mit diesem Modell der Tumorwachstum beobachtet werden. Nach der Deletion von H3.3K27M konnte H3K27me3 wieder detektiert werden.

Zweitens, wurde erfolgreich eine neue Mauslinie etabliert, in welcher die Expression von RFP-getaggtem H3f3b induziert werden konnte. Dies wurde dur die Modifizierung eines bakteriellen artifiziellen Chromosomes (BAC) mit dem H3f3b Gen erreicht, so dass das Fusionsprotein H3f3b-RFP-ERT2 überexprimiert wurde. Mit diesem Konstrukt ist es möglich Histone in lebendigen Zellen und Tieren zu verfolgen.

1. Introduction

1.1. Brain tumors

Glioblastoma multiforme (GBM) shows a low incidence when compared with the most common cancers like lung cancer, breast cancer, colorectal cancer, prostate cancer, stomach cancer and liver cancer. GBM incidence was around 1-2% in 2012 while the six types of cancer mentioned before accounted for 55% of global cases (Ferlay et al., 2015). However, GBM is one of the most common primary malignant brain tumors, with poor prognosis in both adult and children(Ostrom et al., 2014). The overall survival for patients diagnosed with Glioblastoma is 1-2 years (Grossman et al., 2010).

1.1.1. WHO classification

The World Health Organization (WHO) classifies gliomas according to the analysis of differentiation, cell density, nuclear atypia, mitotic activity, microvascular proliferation and necrosis (Ricard et al., 2012) as grade 2 (diffuse infiltrating low-grade gliomas), 3 (anaplastic gliomas), or 4 (glioblastomas) with increasing aggressiveness (**Table 1.1**). GBMs that arise from diffuse astrocytoma (WHO grade II) or anaplastic astrocytoma (WHO grade III) are called secondary GBM (5% of the cases), while *de novo* GBMs (primary GBMs) comprise the remaining 95%(Ohgaki and Kleihues, 2007).

	Phenotype	Grading						Median survival (years)
		Differentiation	Cell density	Nuclear atypia	Mitotic activity	Microvascular proliferation	Necrosis	
Astrocytoma								
Grade 2	Fibrillary or gemistocytic neoplastic astrocytes	Well differentiated	Moderate	Occasional	Generally absent	Absent	Absent	6 to 8
Grade 3	Same as grade 2 astrocytoma	Regional or diffuse anaplasia	Regionally or diffusely increased	Present	Present	Absent	Absent	3
Grade 4	Pleomorphic astrocytic tumour cells	Poor	High	Marked	Marked	Prominent	Present	1 to 2
Oligodendroglioma								
Grade 2	Monomorphic cells, uniform round nuclei, perinuclear halos	Well differentiated	Moderate	Possibly marked	Absent or occasional mitosis	Not prominent	Absent or not conspicuous	12
Grade 3	Same as grade 2 oligodendroglioma	Regional or diffuse anaplasia	Increased	Marked	Usually prominent	Often prominent	Possible	3 to >10
Mixed oligoastrocytoma								
Grade 2	Neoplastic glial cells with astrocytic or oligodendroglial phenotypes	Well differentiated	Moderate	Occasional	No or low	Absent	Absent	6
Grade 3	Same as grade 2 oligoastrocytoma	Anaplasia	High	Marked	High	Might be present	Absent (if present: GBMO)	3

GBMO=glioblastoma with oligodendroglial component.

Table 1: **Histological classification of diffuse gliomas and overall survival**

Table 1.1. Histological classification of diffuse gliomas and overall survival. Reproduced with permission from (Ricard et al., 2012)

1.1.2. Paediatric glioblastoma

Brain tumors represent 20% of all cancer cases in children(Hargrave et al., 2006), and are the first cancer-related cause of death in children(Stiller, 1994). These tumors have a wide variety both histologically and anatomically. One the most diverse brain tumor groups are gliomas; they originate from any place in the Central Nervous System (CNS) and present different histology. Within the gliomas that are located in the brain stem 20% of them comprise low-grade astrocytomas while the remaining 80% arise from the pons and present a diffuse histology(Hargrave et al., 2006). Diffuse intrinsic pontine glioma (DIPG) represents one of the paediatric brain tumors with the worst prognosis; most studies have a median survival of less than one year. Diagnosis nowadays is based on MRI and clinical findings while tissue biopsies are not recommended.

1.1.3. Histology and Pathology

DIPGs are originated in the brain stem and due to the diffusive and infiltrative nature in combination with the location surgical resection is usually not an option (Maria et al., 1993).

Despite all the advances in medicine DIPG treatment has not significantly improved in the last decades. Radiation is the standard of care for the patients but only offers palliative results while chemotherapy has not shown results so far (Hargrave et al., 2006). One probable cause for the failure of treatment improvement is the adaptation of techniques used for adult glioblastoma (Donaldson et al., 2006).

1.2. Chromatin

The length of the DNA molecule in the cell requires it to be packaged in order to fit inside the nucleus. Histones are the proteins in charge of that task and at the same time, they enable the cellular machinery to access the DNA in processes like transcription, recombination, DNA repair and replication. The combination of DNA and all associated proteins is named chromatin. Histone proteins interact with each other and with the DNA to form the basic unit of the chromatin which is the nucleosome. The histone H3 and H4 are combined in a tetramer $(H3\text{-}H4)_2$ and with the addition of two dimers of H2A-H2B they compose the nucleosome. Approximately two turns of the DNA helix (147 base pairs) are wrapped around a nucleosome providing both the necessary packaging and the protection. Despite the primary function as architectural proteins, histones are involved in several cellular processes as DNA repair and chromosome segregation. Chromatin regulation at the level of histones is made mainly by two means: post-transcriptional modifications (PTMs) and the incorporation of histone variants into the nucleosome. PTMs occur preferentially in the histone tail that hangs out of the core of the nucleosome. These modifications include acetylation, methylation, phosphorylation and ubiquitination (Kouzarides, 2007). These PTMs have strong implications for the regulation of transcription and DNA replication and also for the maintenance of the genome stability.

1.2.1. Histone H3.3

In mammalians there are several histone H3 variants. Histones H3.1 and H3.2 are referred to as canonical histone H3 and only differ by one amino acid from each other while there are four additional replacement histones: centromere specific variant CENP-A, H3.3 (Szenker et al., 2011) and testis-specific histones H3.4 (also known as H3t)(Witt et al., 1996) and H3.5 (also known as H3.3C)(Schenk et al., 2011). The primate-specific H3 variants, H3.X and H3.Y can also be added to that list (Wiedemann et al., 2010). Comparing the histone variant H3.3 with its canonical counterpart we can observe differences arising from several levels (**Figure 1.1**).

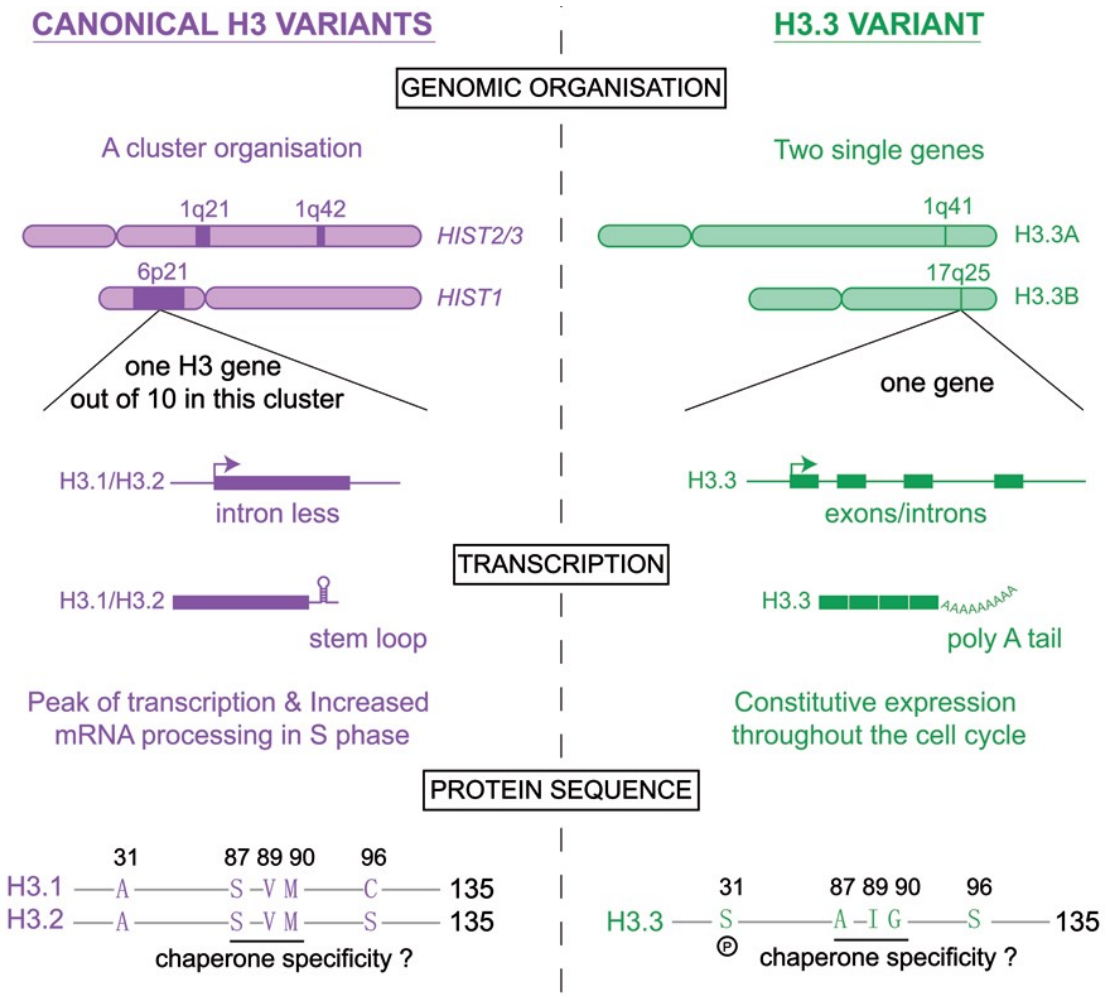

Figure 1.1. Differences between the canonical H3 variants and the histone variant H3.3. Reproduced with permission from (Szenker et al., 2011).

First, in terms of genomic organization the canonical histones H3 are encoded by multiple genes, which cluster together in the genome. The genes encoding the canonical histones H3 don't have introns and their resultant mRNAs are not polyadenylated. Also their translation is highly regulated by the binding of the stem loop binding protein and of the U7 small nuclear RNA to the 3' end of the histone RNAs (Marzluff et al., 2002). These particular genomic and transcriptional characteristics allow a rapid production from the histone H3 canonical genes during the S phase to provide the cell with the necessary pool of H3 protein needed during replication in a DNA synthesis-coupled (DSC) manner. One exception to this is the canonical histone H3.1 which can be incorporated outside of the S phase in the event of DNA repair after UV lesion (Polo et al., 2006). In contrast, the histone variant H3.3 is encoded by only two genes. H3.3A and H3.3B are located in different chromosomes, they have different DNA sequences and regulatory regions but the encoding proteins have exactly the same amino acid sequence (Akhmanova et al., 1995; Frank et al., 2003; Krimer et al., 1993). Opposite to the canonical histone H3, histone H3.3 genes possess introns and the transcribed mRNAs are polyadenylated. Second, histone variant H3.3 can be incorporated into the nucleosomes throughout the whole cell cycle both in a DSC and DSI (DNA synthesis-independent) manner. H3.3 differs in only 4 amino acid differences from H3.2 (at positions 31, 87, 89 and 90) and in five from H3.1 (an additional difference at position 96). Due to the high sequence similarity between H3.3 and the equivalent canonical H3 these particular amino acid differences have been proposed to be responsible for H3.3 distinct characteristics. Residues 87, 89 and 90 are especially interesting in terms of the DSI deposition of H3.3. These three residues are shared among vertebrates and *Drosophila* been Serine, Valine and Methionine for H3 and Alanine, Isoleucine and Glycine for H3.3. Direct mutagenesis of these amino acid residues in *Drosophila* H3 to the corresponding H3.3

residues achieved DSI deposition of H3 (Ahmad and Henikoff, 2002). This finding supports the idea that the pattern SVM (Serine, Valine and Methionine) in H3 is responsible for its restricted deposition. In addition, mutation of the sequence of H3.3B gene to the canonical H3.2 in mouse embryonic stem (ES) cells alters the genome-wide distribution of H3.3 showing that this particular sequence determines its distribution (Goldberg et al., 2010).

1.2.2. Histone H3.3 deposition

Canonical H3 is incorporated into chromatin strictly during S phase in a DSC manner. This process is mediated by two chaperones: antisilencing function protein 1 (ASF1) and chromatin assembly factor-1 (CAF-1) and results in a non-specific and broad genomic distribution. Variant H3.3, which exhibits a DSI deposition, uses two different deposition pathways for the incorporation into the chromatin. The first one is mediated by the histone regulator A (HIRA) complex and targets H3.3 to transcriptionally active genic regions. The second one, death-domain-associated protein/α-thalassemia and mental retardation syndrome X-linked protein (DAXX/ATRX) complex mediates the deposition of H3.3 to pericentromeric, telomeric and repeat regions of the genome (Elsasser et al., 2015; Goldberg et al., 2010; Ray-Gallet et al., 2011). The specific change in residue 90, methionine in the canonical H3 and glycine in the H3.3 variant, allows the formation of a hydrogen bond between H3.3 and DAXX. The point mutation of this residue to glycine but not to alanine permits H3.2 recognition by DAXX (Elsasser et al., 2012). This example shows how important one amino acid can be for the interaction with different chaperone complexes.

1.2.3. Lysine 27 methylation

Whenever both canonical and variant histone H3 are incorporated into the nucleosome the amino terminal end of the protein stays out of the nucleosome core as a tail. This specific disposition of the H3 tail makes it the target of different PTMs affecting the complex regulation of H3 (**Figure 1.2**).

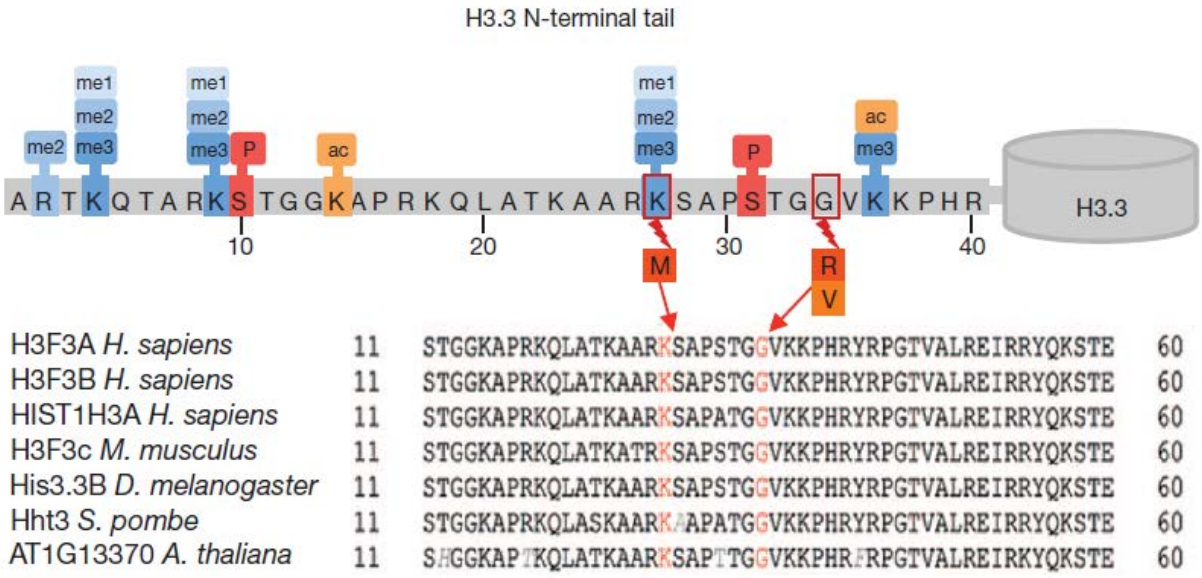

Figure 1.2. Post-translational modifications of the H3.3 tail and multiple alignment of a region of the tail showing the conservation from plants to mammals. Reproduced with permission from (Schwartzentruber et al., 2012)

K27me3 is a PTM associated with transcriptional repression; furthermore enrichment of H3K27me3 correlates with gene silencing (Barski et al., 2007). In addition, results showed that H3K27me3 and the transcription elongation mark H3K36me3 have distinct localizations (Mikkelsen et al., 2007). The methylation of the histone 3 lysine 27 is a process catalyzed by the Polycomb repressive complex 2 (PRC2). The core PCR2 complex is composed by four subunits: EZH1/2, SUZ12, EED and RbAp46/48 and is conserved from *Drosophila* to mammals. PRC2's normal function is to maintain epigenetic gene silencing and X

chromosome inactivation through enzymatic di and trimethylation of the Lysine 27 of the histone H3 (Margueron and Reinberg, 2011).

Additionally to its four subunits PRC2 interacts with AEBP2, PCLs and JARID2. AEBP2 is a zinc-finger protein that interacts with PRC2 to enhance its enzymatic activity (Cao and Zhang, 2004). PCLs (PCL1, PCL2 and PCL3) are the three mammalian orthologues of *Drosophila* PCL. They share the same protein motifs: a tudor domain, two plant homeodomain (PHD) finger domains, a PCL extended domain and a carboxy-terminal domain tail (Wang et al., 2004). PCLs regulate PRC2 enzymatic activity (Nekrasov et al., 2007; Sarma et al., 2008) and gene recruitment of PRC2 (Savla et al., 2008; Walker et al., 2010). JARID2 is a member of the Jumonji family of proteins that catalyzes the demethylation of histone proteins. JARID2 has some conserved regions in its carboxy-terminal end like the ARID domain (potentially a DNA-binding domain), the JmjC and JmjN domains, and a zinc-finger domain. Genome-wide studies have shown that JARID2 is an inhibitor of PRC2 enzymatic activity (Peng et al., 2009; Shen et al., 2009). Different studies on these three additional components of the PRC2 complex have shown that they are not strictly necessary for PRC2 enzymatic activity *in vitro*, however there are required for an optimal activity.

1.2.4. H3.3 function

H3.3 is found across the genome in open chromatin associated with actively transcribed genes and in regions more inactive like telomeres and pericentric chromatin (Shi et al., 2016). This specific genomic distribution supports a role for H3.3 in gene activation and silencing in a context-dependent manner.

1.2.4.1. H3.3 function in chromatin dynamics and transcriptional regulation

The high homology between histone variant H3.3 and the canonical histones H3 makes it unlikely that the incorporation of H3.3 into the nucleosome would affect its stability or structure (Chen et al., 2013; Thakar et al., 2009). Incorporation of H3.3 into the nucleosome regulates chromatin folding causing an open chromatin conformation (Chen et al., 2013). H3.3 counteracts the incorporation of the histone linker H1 altering chromatin compaction as a result. H3.3-enriched regions in *Drosophila* cells have low levels of H1 and upon knockdown of H3.3 these regions increase the levels of H1 (Braunschweig et al., 2009). H3.3 keeps the balance between open and closed chromatin, which is critical for mouse preimplantation development. Loss of H3.3 causes over-condensation and mis-segregation of chromosomes in the two-cell stage leading to aneuploidy (Torres-Padilla et al., 2006). As mentioned before the incorporation of the histone variants H3.3 or H2A.Z does not affect the structure of the nucleosome (Chen et al., 2013; Suto et al., 2000), however nucleosomes containing these two histone variants seem less stable than those containing the canonical versions H3 and H2A (Jin and Felsenfeld, 2007). The instability of these nucleosomes makes them prone to disassembly and facilitates the access of transcription factors and other chromatin-associated factors to the chromatin in human cells (Jin et al., 2009). H3.3 is a mark of transcriptionally activated genes being enriched at promoters, gene bodies and *cis*-regulatory elements. At dynamic regions H3.3 distribution is conserved from yeast to humans (Dion et al., 2007; Ray-Gallet et al., 2011; Rufiange et al., 2007; Schneiderman et al., 2012; Shu et al., 2014; Stroud et al., 2012; Wollmann et al., 2012). Loss of H3.3 genes in *Drosophila* leads to genes both upregulated and downregulated due to transcriptional impairment. Results showed that the genes that were downregulated were mainly highly transcribed genes supporting that H3.3 is required for the transcription of active genes.

Furthermore, H3.3 turnover in promoters and coding regions correlates with polymerase density and transcription level (Jin et al., 2009; Kraushaar et al., 2013). The presence of H3.3 at the promoter region is not limited to active genes; H3.3 can be also found in the promoters of inactive genes probably due to being in a poised state or as reminiscence of previous activation (Mito et al., 2005; Tamura et al., 2009). H3.3 is necessary for the establishment of H3K27me3 at the promoters of developmentally regulated genes in mouse ES cells. H3.3 knockdown results in reduced PRC2 occupancy and H3K27me3 levels but the chromatin landscape of actively transcribed regions like the ones marked with H3K4me3 is not changed (Banaszynski et al., 2013). Despite its association with actively transcribed regions H3.3 has been shown to be incorporated into inactive regions such as telomeres, pericentric chromatin and silent retroviral elements (Drane et al., 2010; Goldberg et al., 2010; Lewis et al., 2010). Altogether, these results point at a complex regulation mechanism of activation and repression of gene expression and of chromatin conformation by H3.3 in a context-dependent manner.

1.2.4.2. H3.3 function during development

H3.3 is a highly conserved histone variant among different species which points at the possibility of it having a conserved function as well. Knockout of both genes, H3.3A and H3.3B, in flies causes complete sterility, transcriptional defects of highly transcribed genes and partial lethality (Sakai et al., 2009). H3.3-deficient flies were affected in the expression of a subset of genes in adults but the timed and localized expression of key developmental genes was not affected (Hodl and Basler, 2009). Knockout models of either H3.3A or H3.3B have shown the importance of H3.3 expression during development. H3.3A knockout mice were viable to adulthood, however males were found to be subfertiles, while H3.3B

homozygous knockout mice showed deficient embryonal growth and did not survive birth. H3.3B heterozygous knockout mice were infertile (Tang et al., 2015). Also, H3.3B knockout in Mouse Embryonic Fibroblast (MEF) cells resulted in karyotype abnormalities, ectopic CENP-A localization and defective chromosome segregation signifying the importance of H3.3 for maintaining chromosome integrity.

H3.3 expression peaks at gastrulation during *Xenopus* development and in the case of a reduction of H3.3 levels gastrulation is arrested and abnormal expression of late mesoderm markers is observed (Ng and Gurdon, 2008). Knockdown of H3.3 in fertilized mouse zygotes produces growth arrest at the morula stage (Lin et al., 2013). H3.3-deficient embryos show a close chromatin phenotype with reduced levels of H3K36me2 and H4K16Ac (open chromatin markers) and increased incorporation of histone linker H1, which results in over-condensation and mis-segregation of the chromosomes (Lin et al., 2013). These results support the hypothesis of H3.3 being in charge of balancing between an open and close chromatin state during early development. Furthermore, the knockout phenotype of HIRA in mice is similar to the observed phenotype in H3.3-deficient *Xenopus* embryos with embryonic lethality and defects in early gastrulation (Roberts et al., 2002; Szenker et al., 2012). DAXX and ATRX knockout mice result in lethality before E9.5 (Garrick et al., 2006; Michaelson et al., 1999). Therefore, HIRA, DAXX and ATRX are essential for early embryonic development but whether this is specifically linked to H3.3 remains to be proven.

1.2.4.3. H3.3 function in cell differentiation

Pluripotent ES cells have the ability to differentiate into multiple lineages as well as self-renewal capacity. This differentiation potential is maintained in ES cells by marking specific genes important for the differentiation into a particular lineage before their expression is induced. In ES cells, the promoters of these lineage-specific genes are marked with H3K4me3 and H3K27me3 modifications. The H3K4me3 mark is usually associated with gene activation while the H3K27me3 mark is associated with gene repression. These regions marked with H3K4me3 and H3K27me3 are called bivalent domains. Results from mouse ES cells show that H3.3 is enriched in these domains (Goldberg et al., 2010). Upon differentiation to neuronal precursor cells (NPCs) the genome-wide distribution of H3.3 changes. Now, those bivalent genes that were activated in NPCs present H3.3 at the transcription starting site (TSS) and the gene body. Opposite to that, bivalent genes that were repressed showed decreased H3.3 at the TSS (Goldberg et al., 2010). In addition, upon knockdown of H3.3 in ES cells the expression patterns of bivalent genes was changed during the differentiation process (Xiong et al., 2016). These findings suggest an essential role for H3.3 in ES cell differentiation, which will need further study to be unraveled.

1.2.4.4. H3.3 function in the brain

Given the fact that histone H3.3 can be deposited throughout the whole cell cycle it is logical to raise the question if H3.3 would function in the same way in post-replicative cells like neurons as it is in dividing cells. Furthermore, the role of H3.3 in transcriptional regulation points at the importance of H3.3 in the developmental brain and in neuronal specialization. Neuronal specialization and plasticity are mediated by activity-dependent changes in gene expression (Greer and Greenberg, 2008). Activity-dependent gene expression can be

regulated by manipulation of the chromatin structure to control the accessibility of the transcriptional machinery to the DNA but the mechanism used to achieve this remains unclear (Borrelli et al., 2008; Maze et al., 2013). Nucleosomal histones have been classically considered highly stable proteins with a slow turnover and half-lives from months to years in post-replicative cells (Commerford et al., 1982). Due to that, former studies in the CNS focused on PTMs and chromatin remodeling as the causes of transcriptional and behavioral plasticity. However, recent results in budding yeast and *Drosophila* showed rapid incorporation of histone variants within active regions of the genome (Deal et al., 2010; Dion et al., 2007) suggesting that rapid nucleosome turnover could affect gene expression in mammalian brain. Classical (Commerford et al., 1982) and recent (Savas et al., 2012; Toyama et al., 2013) analysis of protein stability in rat brain showed a long half-live for H3 over the lifetime of the animal. In addition, studies indicated that H3.3 is accumulated in the brain with age, reaching levels of over 90% of the total H3 pool while canonical H3 levels decreased (Maze et al., 2015; Pina and Suau, 1987)(**Figure 1.3**). These findings point at a different mechanism of chromatin regulation in neurons due to the enrichment of H3.3. Also, different studies support a role for nucleosome dynamics during activity-dependent transcriptional responses in the brain (Maze et al., 2015; Michod et al., 2012; Sun et al., 2015; Zovkic et al., 2014). Specifically, nucleosome turnover has been shown to be necessary for neuronal and glial specific gene expression, synaptic connectivity, dendritic spine formation and maintenance and cognition. H3.3 is incorporated into the nucleosomes by HIRA and removed in a proteasomal-dependent manner which promotes cell-type specific transcriptional responses. Additionally, reduction of H3.3 turnover in neurons impairs the transcription of activity-dependent synaptic genes, reduces dendritic spines, decreases excitatory (glutamatergic) and inhibitory (GABAergic) synapses, and impairs cognition (Maze

et al., 2015; Wenderski and Maze, 2016)(**Figure 1.3**). Another recent study has shown that in mice H3.3 has a role in contextual fear memory and motor learning highlighting the growing importance of H3.3 in the brain lately (McNally et al., 2016). With the increasing appearance of techniques and results the role of H3.3 in brain will eventually grow even more.

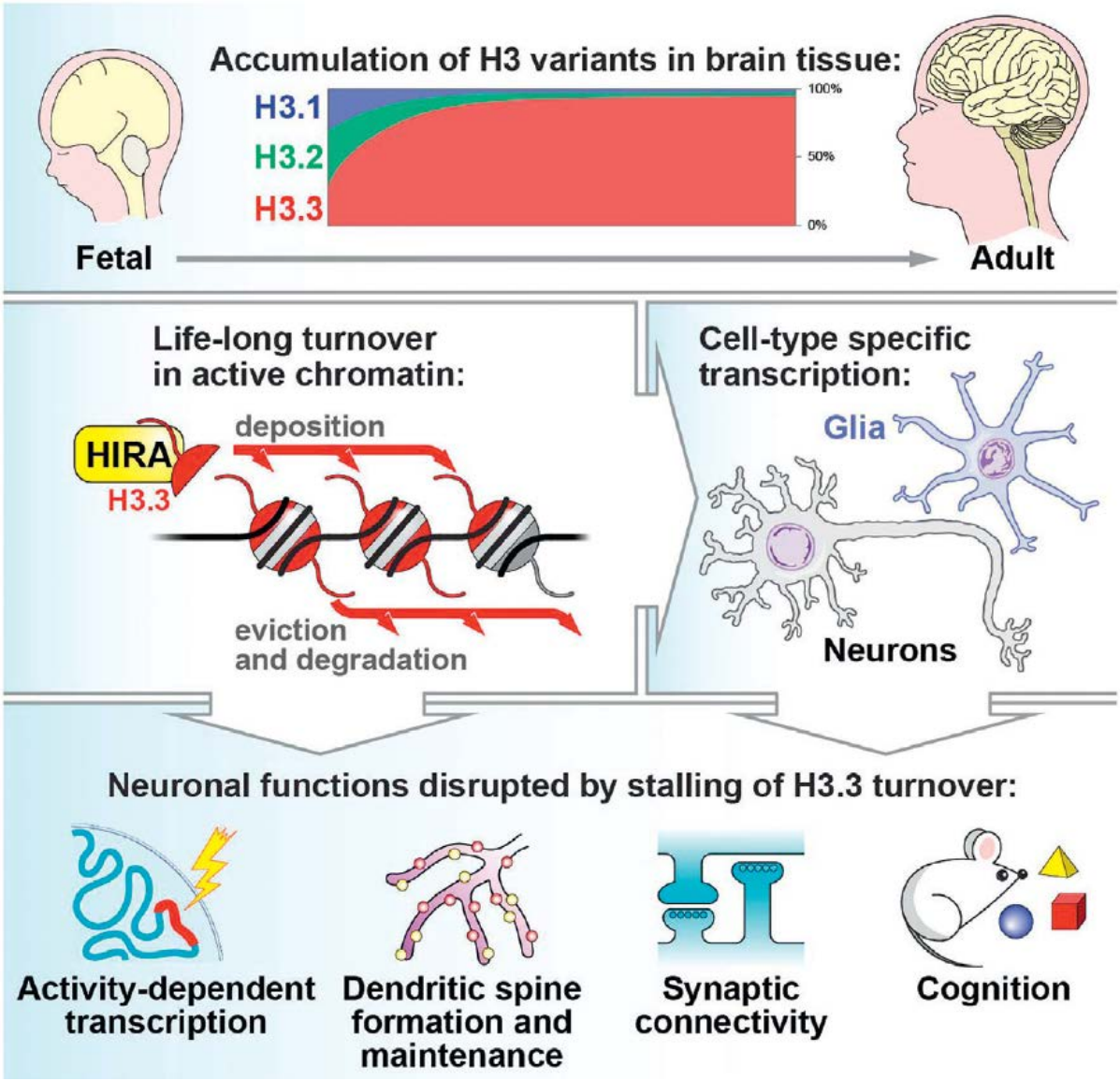

Figure 1.3: Roles for H3.3 turnover in brain. Reproduced with permission from (Wenderski and Maze, 2016)

1.3. Histone H3 mutations in cancer

Recently exome sequencing has identified mutations in H3, which are involved with paediatric GBM and to a lesser degree with adult GBM (Schwartzentruber et al., 2012; Wu et al., 2012). The identified mutations were found in two residues of the H3 tail: lysine 27 was mutated to methionine and glycine 34 was mutated to arginine or valine. Both mutations affect the PTMs of lysine 27 and lysine 36 (Lewis et al., 2013) that have important roles in the regulation of gene expression programs in mammalian cells. Following paediatric glioma, H3 mutations have been already identified in other cancers such as chondroblastoma and giant cell tumors of the bone (Behjati et al., 2013; Maze et al., 2014)(**Table 1.2**). These findings strongly support a role for H3.3 in cancer progression.

Table 2 | **Core histone variants in human disease**

Histone	Number of gene copies	Cell-cycle expression	Mutation and expression pattern	Tumorigenic consequences	Refs
H2A.X	1	RI	Reduced expression	Increased cancer progression in p53-knockout mice	60,61
H2A.Z	2	RI	Over-expression; oncogene	Numerous cancers	121–123
MacroH2A	2	Possibly RI	Reduced expression; tumour suppressor	Melanoma and other cancers	141
H3.1	10	RD	K27M in H3.1B	Adult and paediatric gliomas, including GBMs and DIPGs, respectively	83
H3.3	2	RD and RI	K27M, G34R and G34V in H3.3A	Adult and paediatric gliomas, including GBMs and DIPGs, respectively	82,83
			K36M in H3.3B	Chondroblastoma	101
			G34W and G34L in H3.3A	Giant cell tumours in bone	
CENP-A	1	RI	Over-expression; oncogene	Numerous cancers	115–119

CENP-A, histone H3-like centromeric protein A; DIPG, diffuse intrinsic pontine glioma; GBM, adult glioblastoma; ND, not determined; RD, replication dependent; RI, replication independent.

Table 1.2. Core histones variants in human disease. Reproduced with permission from (Maze et al., 2014)

H3 mutations found in GBM are predominantly in the two genes encoding H3.3 (*H3f3A* and *H3f3B*) and with less frequency in H3.1 genes (*HIST1H3B* and *HIST1H3C*) and are always heterozygous mutations. The specificity and the frequency of these mutations (nearly 80% of

paediatric DIPGs carry the K27M mutation) allow them to be defined as driver mutations in these tumors (Lewis et al., 2013; Vogelstein et al., 2013).

The mutations are region-specific, with the K27M mutation occurring predominantly in a midline region (brain stem, spinal cord and thalamus) and G34R/V is found in the cerebral cortex. There is also an age difference in the appearance of these tumors, being the median age of diagnosis for K27M of 10.5 years while G34R/V is diagnosed at a median age of 18 years (Sturm et al., 2012). These data suggest the implication of an early neuronal precursor cell (NPC) acquiring the mutation as a first step in the formation of these gliomas. The consequence of the K27M mutation is the dominant inhibition of the enzymatic activity of the PRC2 complex both in *cis* and *trans* resulting in the decrease of the H3K27me3 repressive mark in the whole cell as well as a modest increase in H3K27Ac (Lewis et al., 2013). Genome-wide studies of the H3K27me3 pattern and the gene expression in K27M patient samples showed global reduction of H3K27me2, H3K27me3 and DNA methylation. Surprisingly, H3K27me3 and EZH2 were found to be locally increased in hundreds of gene loci (Bender et al., 2013; Chan et al., 2013) related with various cancer pathways. These results strongly suggest that the K27M mutation reshapes the epigenetic landscape and the gene expression of the cell through changes in H3K27me3 and DNA methylation.

The H3.3K27M protein strongly precipitates with EZH2, suggesting an interaction between the EZH2 active site and K27M (Chan et al., 2013). Furthermore, *in vitro* studies have shown that a K27M peptide is enough to block PRC2 activity (Brown et al., 2014; Lewis et al., 2013). K27M inhibition of PRC2 activity is equivalent to GSK343 inhibition, a well-known chemical EZH2 inhibitor (Bender et al., 2013). The use of a brain stem mouse glioma model based on the overexpression of the platelet-derived growth factor (PDGF) in combination with the expression of H3K27M was sufficient to significantly decrease H3K27me3 and increase

H3K27Ac (Lewis et al., 2013). In addition, the combination of a p53 mutation and H3K27M expression in Nestin expresing progenitor cells in the neonatal mouse brain did not induce gliomas but was enough to induce proliferating ectopic cell clusters in 72% of the mice while H3.3 wildtype expression in combination with a p53 mutation was not sufficient to induce proliferating ectopic cell clusters (Lewis et al., 2013). However, K27M expression in undifferentiated human ES cells or in primary human astrocytes did not induce proliferation (Funato et al., 2014) pointing at a cell type and developmental stage specificity for the K27M phenotype. A recent study, involving the use of a mouse model consisting in NSC expressing PDGFB and tagged H3.3K27M in addition to primary patient-derived DIPG cell lines showed that H3.3K27M potentiates tumorigenesis as well as that the residual PRC2 activity is required for the proliferation of H3.3K27M-expressing DIPGs (Mohammad et al., 2017). In addition, the data from the study supported the potential of EZH2 as a therapeutic target in these tumors.

Combined efforts in sequencing of paediatric and adult GBM have raised some light into the complexity of these tumors. As a consequence different subgroups of gliomas have been proposed based on criteria like coexisting mutations, methylation patterns or gene expression analysis (Jones and Baker, 2014; Sturm et al., 2012)(**Figure 1.4**). The K27 subgroup is characterized by the K27M mutation and includes tumors from almost exclusively midline locations as DIPGs and some rare tumors in the basal ganglia and the spinal cord. Additionally, the K27 subgroup shows a significantly lower expression of the ventral telencephalic marker FOXG1 than other subgroups. Opposite to the G34 subgroup, the K27 subgroup also displayed OLIG2 expression, a marker for diffuse gliomas (Ligon et al., 2004). Furthermore, OLIG2-positive progenitor-like cells of the subventricular zone (SVZ) have been suggested as potential glioma-initiating cells (Wang et al., 2009). The specificity of

the H3K27M mutation in terms of tumor location and different expression of neuronal lineage markers suggests a difference in the cell of origin of these tumors which still remains to be proven.

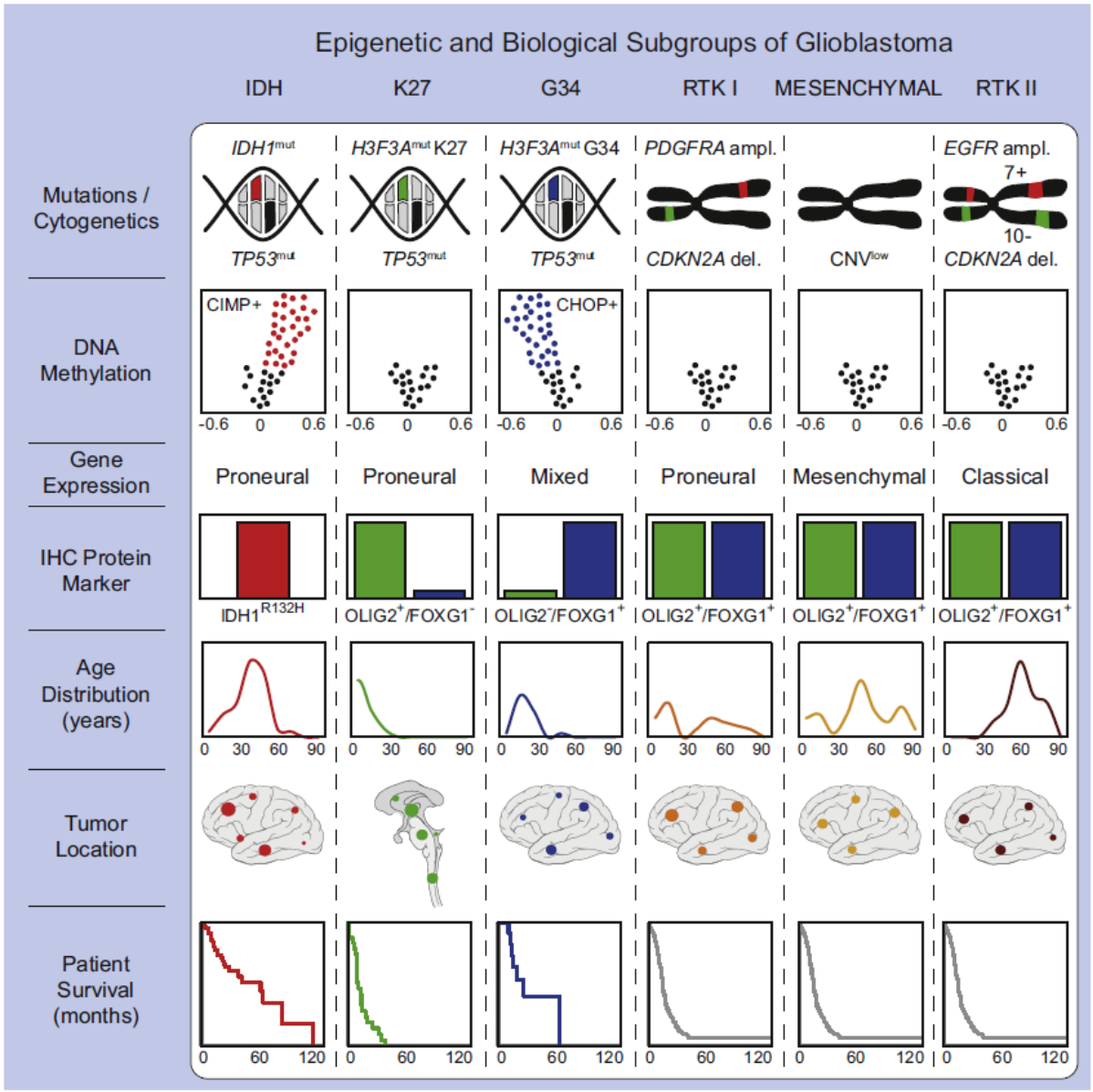

Figure 1.4. Summary of key molecular and biological characteristics of GBM subgroups. Reproduced with permission from (Sturm et al., 2012).

Sequencing results have shown that paediatric GBMs present frequent alterations in the canonical cancer pathways also altered in adult GBM, the receptor tyrosine kinase (RTK)-RAS-PI3K pathway, the TP53 pathway and the RB pathway (Cancer Genome Atlas Research, 2008; Parsons et al., 2008). However, the specific members of the pathways mutated are

different between adult GBMs and paediatric GBMs (Sturm et al., 2014)(**Figure 1.5**). Concerning the (RTK)-RAS-PI3K pathway, paediatric GBMs present mutations in the genes PIK3R1 and PIK3CA. These genes encode the regulatory and catalytic subunits p85 and p110α of the PI3Kα, respectively. Homozygous mutations of the tumor suppressor gene PTEN are rare but present in paediatric GBMs and cause a loss-of-function phenotype. The most common member of the pathway mutated in paediatric GBMs is the platelet-derived growth factor receptor-α (PDGFRA) being amplified and/or mutated in around 30% of the cases (Jones and Baker, 2014). Additionally, the mesenchymal epithelial transition factor (MET) and the insulin-like growth factor 1 receptor (IGF1R) are also found mutated in paediatric GBMs (Bax et al., 2010; Paugh et al., 2011; Paugh et al., 2010; Puget et al., 2012; Qu et al., 2010). Mutations in TP53 are present in approximately 55% of paediatric GBMs (Buczkowicz et al., 2014; Schwartzentruber et al., 2012; Wu et al., 2014) with also 9-23% of mutations in DIPGs affecting the gene PPM1D which has a role downstream of p53 in the DNA damage response (Wu et al., 2014). Finally, the RB pathway is considerably less mutated in paediatric GBMs than in adult GBMs. Homozygous deletion of cyclin-dependent kinase inhibitor 2A (CDKN2A) are rare in DIPGs but are represented in 25% of non-brain stem paediatric gliomas. Additionally, amplification of CDK4, CDK6 or CCND1 (Cyclin D1), CCND2 or CCND3 (all of them components of the cyclin-CDK complex in charge of the phosphorylation of RB at the G1 checkpoint) are found mutated in paediatric brain tumors from both the brain stem and the cortex (Bax et al., 2010; Paugh et al., 2011; Qu et al., 2010).

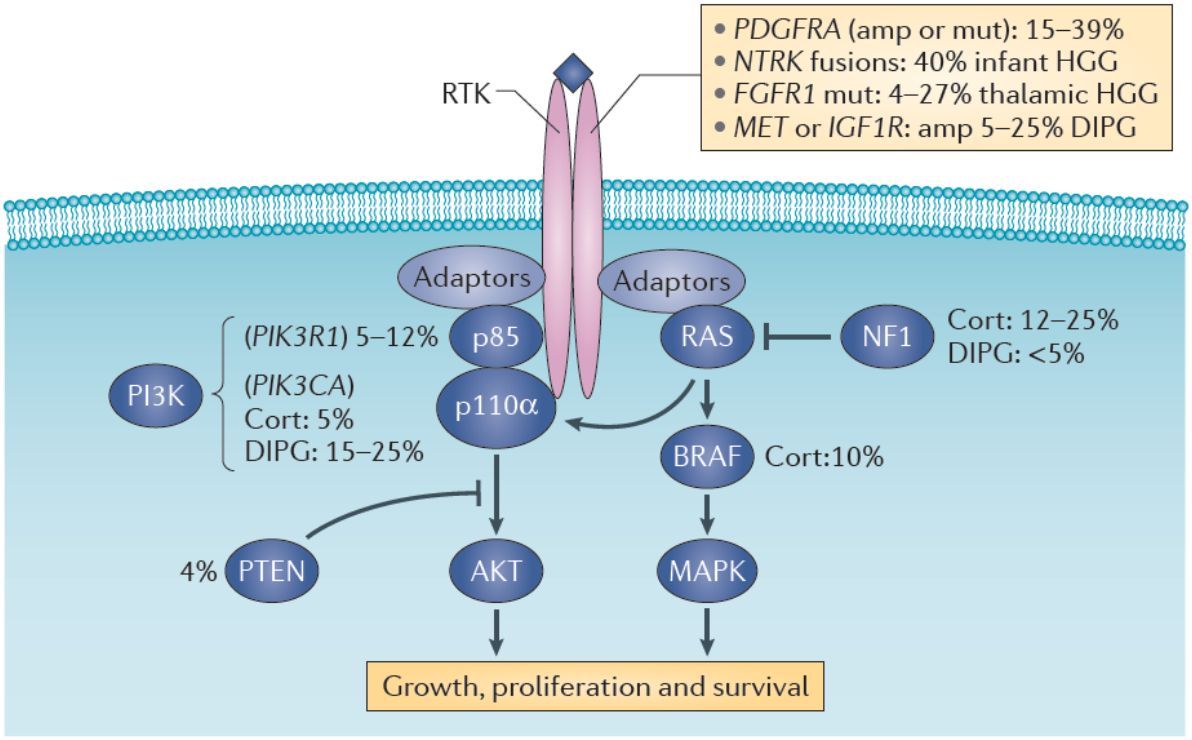

Figure 1.5. Recurrent mutations activate PI3K and MAPK signalling pathways in paediatric high-grade glioma. Reproduced with permission from (Jones and Baker, 2014).

1.4. High grade brain tumor model

1.4.1. RCAS-TVA system

The Replication-Competent Avian sarcoma-leukosis Virus (ASLV) with long terminal repeats (LTR) and splice acceptor (RCAS) vectors has been used for the introduction and expression of genes in both cell culture and animal model systems. The RCAS vectors have the ability to infect cells that have the avian receptor tv-a(Bates et al., 1998; Bates et al., 1993) and which are actively dividing(Fritsch and Temin, 1977; Humphries et al., 1981; Varmus et al., 1977). The RCAS-TVA system has been used to express genes in transgenic mice, which have been introduced with the tv-a receptor under the control of a cell lineage-specific promoter to generate murine models of specific cancers (Fisher et al., 1999; Holland and Varmus, 1998).

Contrary to other oncogenic viruses the RCAS vector contains a full complement of viral genes plus the oncogene src.

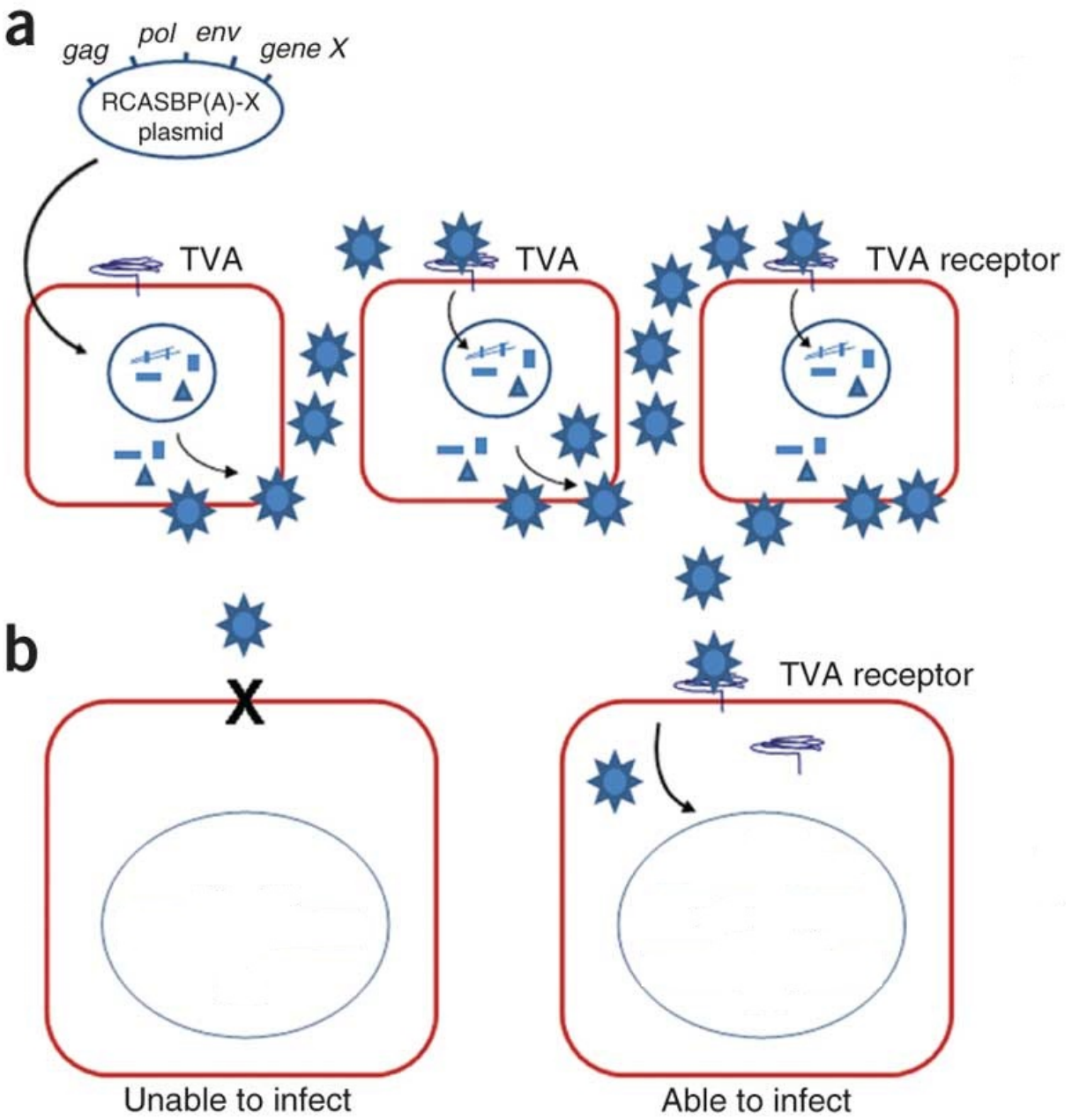

Figure 1.6. Production of avian retroviruses and tissue-specific somatic retroviral gene transfer in vivo using the RCAS/TVA system.

Adapted with permission from (von Werder et al., 2012)

Taking advantage of this the src gene can be substituted by an endogenous sequence and maintain its replication capability (Oh et al., 2002). This method has been used for the induction of brain tumors in mice using Nestin-tva transgenic mice and the overexpression of a combination of oncogenes through the RCAS vector (**Figure 1.6**)(Hughes, 2004). Upon

intracranial injection of the virus particles into the SVZ of newborn mice, Nestin-expressing cells, which are the neural progenitor cells, are infected with the combination of RCAS vectors. The brain tumors generated by this method highly mimic the histology of the human brain tumors (Huse et al., 2013; Huse and Holland, 2009). The combined expression of PDGFB and a constitutively active AKT produced 100% gliomas of which 60% were high-grade GBMs (Zhu et al., 2014).

2. Aim

DIPG is one of the leading cancer-related causes of death in children and its treatment has not seen any improvement over the last decades. However, recent studies have spread some hope in changing this situation due to the growing amount of knowledge uncovered. Our lab developed a robust HGG model making use of the RCAS/TVA system. The aim of this study is to establish a mouse model for DIPG utilizing our current mouse model. This will include:

- introduction of the tagged H3.3/K27M flox into our existing HGG model
- validation of the model by histology analysis, marker expression (loss of H3K27me3 and recovery of H3K27me3 upon tamoxifen treatment)
- in vivo tumor growth monitoring by BLI
- optimization of the mouse model by relocation of the induction site to the pons

Over the last years several studies have linked H3.3 with important roles in the brain like contextual fear memory, motor learning, cognition and synapses. Furthermore, histone H3.3 turnover has been proposed to have a greater role due to the H3.3 pool reaching over 90% of the total H3 in the adult brain. In order to contribute, this study aims to develop tools to study H3.3 activity in the brain:

- histone H3.3 tracing in living behaving animals
    - establishment of a mouse line over-expressing an inducible GFP tagged H3f3a
    - establishment of a mouse line over-expressing an inducible RFP tagged H3f3b

3. Materials and Methods

3.1. Buffers and solutions

A "MilliQ Water Purification System" (Millipore) was used for the preparation of aqueous solutions.

Solution	Composition
4% PFA (pH 7.4)	4 gr paraformaldehyde in 100 ml PBS
DNA Loading buffer (10 ml)	9.5 ml Formamide, 5 mg bromophenolblue, 5 mg xylencyanol 0.5 mg of 0.5 M EDTA
Eosin (0.1%)	Eosin (0.5%) diluted 1:5 in 70% ethanol plus 5 drops of Glacial Acid
Injection Buffer	10mM Tris-HCL pH 7.5, 0.1mM EDTA (pH 8.0), 100mM NaCl, H_2O Aqua ad iniectabilia Braun
NID-buffer/500ml	25ml 1M KCl, 5ml 1M Tris-HCl PH8.3, 1ml 1M MgCl2, 0.5ml 100mg/ml gelatin, 22.5ml 10%NP4O, 22.5ml 10%Tween20, 424ml H2O, add 1% ProteinaseK (10mg/ml) freshly
PBST (Triton X-100)	PBS containing 0.1% Triton X-100
PBST (Tween 20)	PBS containing 0.1% Tween 20
Phosphate buffered saline (PBS)	137 mM NaCl, 2.7mM KCL, 9.2 mM Na2HPO4, 1.8Mm KH2PO4
TE (Tris-EDTA)	10 mM Tris/HCl pH 8.0, 1 mM EDTA

Table 3.1. List of buffers and solutions.

3.2. Cell culture reagents

Reagent (Catalog number)	Supplier
Accutase (A6964-100ML)	Sigma Aldrich, USA
Dulbecco's Modified Eagle's Medium (30-2002)	ATCC, UK
FBS (30-2020)	
Fugene HD Transfection Reagent (E2311)	Promega, Germany
Penicillin/Streptomycin (15140122)	Gibco Invitrogen, USA
Phosphate Buffered Saline (14190250)	

Table 3.2. List of cell culture reagents.

3.3. General Reagents

Reagent (Catalog number)	Supplier
Agarose for PFGE (A2929-25G)	Sigma Aldrich, USA
CHEF DNA Size Standard-Lambda Ladder (1703635)	BioRad, USA
Concentrated Antigen Retrieval Citra Solution (HK086-9K)	Biogenex, USA
Diaminobenzidine tablets (D4293-50SET)	Sigma Aldrich, USA
dNTP Mix 10MM 1ml (10319879)	Thermo Scientific, USA
Ethidium Bromide (1239-45-8)	BioRad, USA
GelRed in water (10000X) (M3199.5000)	Genaxxion, Germany
Hydrogen peroxide 30% (A1134-1000)	Applichem, Germany
L-Arabinose (A3300)	USBiological, USA
MassRuler Express Reverse DNA Ladder Mix (SM1293)	Fermentus, USA
Millipore Membran VMW PO2500 / VM 0.025µm	Millipore, USA
Normal Swine Serum (X0901)	Dako, USA
Pap Pen Immunostaining Pen (MKP-1)	Kisker Biotech, Germany
PFA (0335.3)	Roth, Germany
Sunflower Seed oil (S5007-1L)	Sigma Aldrich, USA
VECTASTAIN ABC HRP Kit (PK-4000)	Vector Laboratories, USA
X-tracta disposable gel extraction tool (N2000-0100)	Starlab, UK

Table 3.3. List of general reagents.

3.4. Drugs

Drug	Supplier
Ampicillin (A1593)	Sigma Aldrich, USA
Chloramphenicol (C0378)	
Tamoxifen free base (T5648-5G)	
Isoflurane (47006XN)	IsoFlo, Germany

Table 3.4. List of drugs.

3.5. Instruments

Instrument	Supplier
Bio-rad CHEF-DR III System	BioRad, USA
Bio-rad gene pulser electroporator	
Centrifuge 5424R	Eppendorf, Germany
Centrifuge 5804R	
Ecotron	Infors-HT, Switzerland
Heating block QBT	Grant Instruments , UK
IVIS Lumina II In Vivo Imaging System	Perkin Elmer, USA
Leica RM 2255 microtome	Leica, Germany
Multitron pro	Infors-HT, Switzerland
NanoDrop ND-1000 spectrometer	NanoDrop, USA
ProFlex PCR System	Thermo Fisher, USA
Ultraspec III spectrophotometer	Pharmacia (Pfizer), USA
UV Gel Documentation	BioRad, USA
Zeiss Axiophot	Zeiss, Germany
Zeiss Axioskop 40 microscope	
Zeiss Cellobserver	
Zeiss LSM 700/780/880	

Table 3.5. List of instruments.

3.6. Kits

Kit (Catalog number)	Supplier
Centrifugal Filter Units (MRCF0R030)	Millipore, USA
D-Tube Dialyzer Maxi, MWCO 12-14 kDa (71510-3)	
Kapa2g Fast Readymix with Dye (KAPBKK5101-03)	KAPA Biosystems, USA
QiaQuick gel extraction Kit (28706)	Qiagen, Germany
QiaPrep mini prep Kit (27106)	
QIAGEN Large-construct Kit (12462)	
QIAGEN Plasmid maxi Kit (12163)	
Vectashield® Hard+Set Mounting Medium (H-1400)	Linaris, Germany

Table 3.6. List of kits.

3.7. Vectors

Vector	Supplier
H3f3a BAC (RP24-252A14)	BACPAC Resources Center, Children's Hospital Oakland Research Institute, California, USA
H3f3b BAC (RP24-205P9)	
H3f3a-GFP-ERT2 BAC	Modified from H3f3a BAC
H3f3b-RFP-ERT2 BAC	Modified from H3f3b BAC
pcDNA3.1(+)	Thermo Fisher Scientific, Germany
pIndu-creERT2	Gunther Schütz, DKFZ, Germany
pIndu-GFP-ERT2	Modified from pIndu-creERT2
pIndu-RFP-ERT2	
RCAS-AKT	Eric C. Holland, Memorial Sloan-Kettering Cancer Center, New York, USA
RCAS-GFP	Eric C. Holland, Memorial Sloan-Kettering Cancer Center, New York, USA
RCAS-H3.3-GFP	Modified from RCAS-AKT
RCAS-K27M-GFP	
RCAS-PDGFB	Eric C. Holland, Memorial Sloan-Kettering Cancer Center, New York, USA

Table 3.7. List of vectors.

3.8. Antibodies

Antibody (Dilution; Catalog number)	**Supplier**
Chicken anti-GFP (1:1000 IF/IHC, ab13970)	Abcam, UK
Mouse anti-PCNA (1:400 IF; NA03)	Calbiochem, USA
Rabbit anti-Ki67 (1:500 IF, 1:1000 IHC; ab15580)	Abcam, UK
Rabbit anti-H3K27me3 (1:1000 IF, 1:200 IHC; 9733s)	Cell Signaling, USA
Rabbit anti-H3K27me3 (1:200 IHC; pAb-069-050)	Diagenode, Belgium
Goat anti-Chicken Biotinylated (1:400; BA9010)	Vector Laboratories, USA
Goat anti-Rabbit Biotinylated (1:400; BA1000)	
Donkey anti-Rabbit Alexa 594 (1:400; A21207)	Life Technologies, USA
Goat anti-Chicken Alexa 488 (1:400; A11039)	
Goat anti-mouse Alexa 633 (1:400; A21050)	

Table 3.8. List of antibodies.

3.9. Enzymes

Enzyme	**Supplier**
Proteinase K (A3830,0025)	AppliChem, Germany
Phusion High-Fidelity DNA Polymerase (M0530S)	New England Biolabs, USA
T4 DNA Ligase (M0202S)	
AgeI-HF (R3552S)	
BamHI (R0136T)	
BamHI-HF (R3136T)	
ClaI (R0197S)	
EcoRI (R0101S)	
EcoRV (R0195S)	
EcoRV-HF (R3195S)	
HindIII (R0104S)	
KpnI (R0142S)	
MluI-HF (R3198S)	
NheI (R0131S)	
NheI-HF (R3131S)	
NotI (R0189S)	
NotI-HF (R3189S)	
PmeI (R0560S)	
SnaBI (R0130S)	
SwaI (R0604S)	
XbaI (R0145S)	
XhoI (R0146S)	

Table 3.9. List of enzymes.

3.10. Oligonucleotides

Product name		Sequence	Product Size (bp)
H3f3a left homology arm	Forward Reverse	5'-GCCTCAGGTACCTACGTAAGGATGAGGACG-3' 5'-CAGTCGTAGCGGCCGCAGCACGTTCTCCGCG-3'	403
H3f3a right homology arm	Forward Reverse	5'-TCAGGATCTCTAGATAAGAGTCCACTATG-3' 5'-TCCTATGCTAGCTACGTATAGTGAATGGAT-3'	443
GFP (pIndu)	Forward Reverse	5'-ATTAATATGCGGCCGCTGCGGTACCGCGGGCC-3' 5'-GCAGATGGCTCGAGATCGCCCTTGTACAGCTCGTC-3'	790
H3f3b left homology arm	Forward Reverse	5'-GCCTCAGGTACCTACGTAGGCAGAGGGCTG-3' 5'-CACTCCTAGGATCCAGCTCTCTCCCCCCG-3'	501
H3f3b right homology arm	Forward Reverse	5'-TGAGGATATCTAGATAAGTTGAAGCGGTT-3' 5'-TCCTATGCTAGCTACGTATGGTTAAACACT-3'	400
RFP (pIndu)	Forward Reverse	5'-TTGCTGTTGGATCCGACAACACCGAGGAC-3' 5'-CTACATCACTCGAGATCGCCCTGGGAGCCGGAGTG-3'	706
H3.3-GFP loxp and K27M-GFP loxp	Forward Reverse	5'TACGGCCGCGGCCGCATAACTTCGTATAGGATACCTTATA CGAAGTTATATGGCACGTACCAAGC-3' 5'ACATCGCATCGATATAACTTCGTATAAGGTATCCTATACGA AGTTATTTACTTGTACAGCTCGTC-3'	1257
H3f3b wt band	Forward Reverse	5'-CACTCTTCCCATTCATCCTG-3' 5'-CATGCCCAAAGACATCCAGT-3'	199
H3f3b mt band	Forward Reverse	5'-GGACAGCTTCATGTAGTCGG-3' 5'-CATGCCCAAAGACATCCAGT-3'	310
H3f3a wt band	Forward Reverse	5'-TTTCCCCTCATAGTGGACTC-3' 5'-GTTCCAATACACTTCCTCTG-3'	415
H3f3a mt band	Forward Reverse	5'-AGCATGCCTGCTATTGTC-3' 5'-CCATGATCAGGTCCACCTTC-3'	915

Table 3.10. List of oligonucleotides with their product name and size.

3.11. Animal housing and Tamoxifen (TAM) treatment

The animals were housed according to international standard conditions and all animal experiments confined to local and international guidelines for the use of experimental animals. Nestin-Tva mouse line was kindly provided by Eric Holland. Nestin-CreERT2 mouse line was generated as described elsewhere. The line has been successfully used to target both SVZ and SGZ NSCs via TAM injection (Liu et al., 2008; Liu et al., 2010). TAM (Sigma) was

dissolved in sunflower seed oil (Sigma) with 10% pure Ethanol to prepare a 10mg/ml solution. Intraperitoneal injection was performed as 1mg/day for 10 days. The health of the animals was monitored every day and was scored according to criteria in **Table 3.11**. After reaching a score of 10 animals were monitored at least twice per day and upon reaching a score of 20 animals were sacrificed.

Category	**Observation**	**Points**
Body weight	Unaffected or increased	0
	Weight reduction <5%	1
	Weight reduction 5-10%	5
	Weight reduction 10-20%	10
	Weight reduction >20%	20
General condition	Smooth skin; Body openings clean; Eyes clear	0
	Fur defects (reduced or exaggerated body care)	1
	Fur blunt, disorganized, unkempt body openings, eyes cloudy; Increased muscle tone, slight hydrocephaly	5
	Dirty skin, glued or moist body openings, abnormal posture, opaque eyes; High muscle tone	10
	Cramps, paralysis (trunk muscles, extremities); Breathing; Animal feels cold; Severe hydrocephaly	20
Spontaneous behaviour	Normal behavior (sleeping, reaction to blows and touch, curiosity, social contacts)	0
	Slight deviations from normal behavior	1
	Unusual behavior, restricted motor function or hyperkinetics	5
	Self-isolation, lethargy; Pronounced hyperkinetics or behavioral stereotypes; coordination disorders	10
	Painfulness when grabbing; Self - amputation (autoaggression)	20

Table 3.11. Criteria to euthanize experimental animals.

3.12. Polymerase Chain Reaction

Polymerase Chain Reactions were performed using either a Kapa2g Fast Readymix with Dye kit or a mix containing Phusion High-Fidelity DNA Polymerase. The PCR mix reagents and their reaction conditions are listed in **Table 3.12**, **3.13** and **3.14**, respectively.

Kapa2g PCR	**Volume**
2X Kapa2g Fast Readymix with Dye	7 µl
Forward primer (10 pmol)	0.5 µl
Reverse primer (10 pmol)	0.5 µl
DNA	2 µl
H_2O	4 µl
Total	**14 µl**

Table 3.12. PCR program for Kapa2g reaction.

Phusion PCR	**Volume**
Phusion High-Fidelity DNA polymerase	0.2 µl
5X Phusion High-Fidelity DNA polymerase Buffer	3 µl
dNTPs	2 µl
Forward primer (10 pmol)	1 µl
Reverse primer (10 pmol)	1 µl
DNA	2 µl
H_2O	5.8 µl
Total	**15 µl**

Table 3.13. PCR program for Phusion reaction.

<table>
<tr><th>Product Name</th><th>Initial Denaturation</th><th>Denaturation</th><th>Annealing</th><th>Extension</th><th>Cycle number</th><th>Final Extension</th></tr>
<tr><td>H3f3a left homology arm</td><td rowspan="13">94°C, 5 min</td><td rowspan="13">94°C, 30 sec</td><td rowspan="5">64°C, 30 sec</td><td rowspan="4">72°C, 30 sec</td><td rowspan="13">35</td><td rowspan="13">72°C, 10 min</td></tr>
<tr><td>H3f3a right homology arm</td></tr>
<tr><td>H3f3b left homology arm</td></tr>
<tr><td>H3f3b right homology arm</td></tr>
<tr><td>GFP (pIndu)</td><td rowspan="3">72°C, 45 sec</td></tr>
<tr><td>RFP (pIndu)</td></tr>
<tr><td>H3.3-GFP loxp</td><td rowspan="3">56°C, 30 sec</td></tr>
<tr><td>K27M-GFP loxp</td></tr>
<tr><td>H3f3a BAC wt band</td><td>72°C, 30 sec</td></tr>
<tr><td>H3f3a BAC mt band</td><td>58°C, 30 sec</td><td>72°C, 1 min</td></tr>
<tr><td>H3f3b BAC wt band</td><td>56°C, 30 sec</td><td rowspan="2">72°C, 45 sec</td></tr>
<tr><td>H3f3b BAC mt band</td><td>58°C, 30 sec</td></tr>
</table>

Table 3.14. PCR conditions.

3.13. Enzymatic restrictions

Template (µl)	Product	Length (bp)	Enzyme 1 (µl)	Enzyme 2 (µl)	Buffer (µl)	BSA (µl)	H_2O (µl)
pIndu creERT2 (2.3) (3 µg)	pIndu creERT2	5498	NheI (1)	n/a	NEBuffer 2 (5)		41.7
H3f3a right arm PCR (2) (1 µg)	H3f3a right arm	425	XbaI (0.5)	NheI (0.5)	NEBuffer 2 (2)		15
H3f3b right arm PCR (2.3) (1 µg)	H3f3b right arm	382					14.7
pcDNA 3.1+ (3.1) (3 µg)	pcDNA 3.1+	5428	NotI-HF (1)	KpnI (1)	NEBuffer 2 (5)		39.9
H3f3a left arm PCR (2.4) (1 µg)	H3f3a left arm	385	NotI-HF (0.5)	KpnI (0.5)	NEBuffer 2 (2)		14.6
pcDNA 3.1+ (3.1) (3 µg)	pcDNA 3.1+	5428	BamHI-HF (1)	KpnI (1)	NEBuffer 1 (5)		39.9
H3f3b left arm PCR (1.8) (1 µg)	H3f3b left arm	483	BamHI-HF (0.5)	KpnI (0.5)	NEBuffer 1 (2)		15.2
pcDNA 3.1+ H3f3a left arm (2.3) (1 µg)	pcDNA 3.1+ H3f3a left arm	5748	NotI (0.5)	XhoI (0.5)	NEBuffer 3 (2)		14.7
GFP PCR (1.5) (1 µg)	GFP	770					15.5
pcDNA 3.1+ H3f3b left arm (2.5) (1 µg)	pcDNA 3.1+ H3f3b left arm	5897	BamHI (0.5)				14.5
RFP PCR (2.1) (1 µg)	RFP	686					14.9
pIndu creERT2 (2.3) (3 µg)	ERT2	959	BamHI (1)	XhoI (1)	NEBuffer 3 (5)		40.7
pIndu creERT2 H3f3a right arm (2) (2 µg)	pIndu H3f3a right arm	4310	HindIII (1)	BamHI (1)	NEBuffer 3 (2)		14
pcDNA 3.1+ H3f3a left arm-GFP (2.1) (1 µg)	H3f3a left arm-GFP	1155	HindIII (0.5)	XhoI (0.5)	NEBuffer 2 (2)		14.9
pIndu creERT2 H3f3b right arm (1.8) (2 µg)	pIndu H3f3b right arm	4363	KpnI (1)	BamHI-HF (1)	NEBuffer 1 (2)		14.2
pcDNA 3.1+ H3f3b left arm-RFP (2.6) (1 µg)	H3f3b left arm-RFP	1161	KpnI (0.5)	XhoI (0.5)			14.4
H3f3a BAC (3.5) (5 µg)	Band pattern	Several	EcoRV (1)	ClaI (1)	CutSmart (3)		21.5
H3f3b BAC (4) (5 µg)							21

pIndu H3f3a-GFP-ERT2 (1.1) (1.5 µg)	H3f3a arms-GFP-ERT2	4019	SnaBI (1)	n/a	CutSmart (2)	n/a	15.9
pIndu H3f3b-RFP-ERT2 (1.5) (1.5 µg)	H3f3b arms-GFP-ERT2	3991					15.5
H3f3a arms-GFP-ERT2 (30) (0.75 µg)	H3f3a arms-GFP-ERT2	4019			CutSmart (4)		5
H3f3b arms-GFP-ERT2 (30) (0.80 µg)	H3f3b arms-GFP-ERT2	3991					5
H3f3a-GFP-ERT2 BAC (3) (5 µg)	Band pattern	Several	EcoRV-HF (1)	XhoI (1)	CutSmart (5)		40
H3f3b-RFP-ERT2 BAC (2.3) (5 µg)	Band pattern	Several	BamHI (1)		NEBuffer 3 (5)		40.7
H3f3a-GFP-ERT2 Amp$^-$ BAC (3.5) (5 µg)	Band pattern	Several	AgeI-HF (1)	n/a	CutSmart (5)		40.5
H3f3b-RFP-ERT2 Amp$^-$ BAC (4) (5 µg)	Band pattern	Several	NheI-HF (1)				41
H3f3a-GFP-ERT2 Amp$^-$ BAC (35) (50 µg)	Linearized H3f3a BAC	Several	PmeI (5)		CutSmart (10)		50
H3f3b-RFP-ERT2 Amp$^-$ BAC (40) (50 µg)	Linearized H3f3b BAC	Several	MluI-HF (5)	SwaI (5)	NEBuffer 3 (10)		40
pBabe H3.3 (1) (1 µg)	H3.3	411	EcoRI (0.5)	BamHI (0.5)	NEBuffer 3 (2)	2	14
pBabe H3.3K27M(1) (1 µg)	K27M	411					
p-eGFP-N1 (1.2) (2 µg)	p-eGFP-N1	4700					13.8
H3.3-GFP loxp PCR (2.1) (1 µg)	H3.3-GFP loxp	1237	ClaI (0.5)	NotI (0.5)	NEBuffer 2 (2)	0.5	14.4
K27M-GFP loxp PCR (2.3) (1 µg)	K27M-GFP loxp	1237					14.2
RCAS-Akt (1.8) (3 µg)	RCAS	10000	ClaI (1)	NotI (1)			13.7

Table 3.15. Enzymatic restrictions conditions.

3.14. DNA Ligation

DNA ligation reactions were incubated for 4 hours at room temperature. The amount of DNA was calculated to maintain a ratio of 1:3 between the vector and the insert; with the vector being 50 fmol and the insert 150 fmol. The reaction volumes for each ligation are shown in **Table 3.16**.

Ligation		**Vector**	**Insert DNA (µl)**		**10X Ligation**	**T4 DNA**	**H_2O**
Vector	**Inserts**	**DNA (µl)**	**1**	**2**	**Buffer (µl)**	**Ligase (µl)**	**(µl)**
pIndu creERT2 (NheI cut)	Control	4	n/a	n/a	2	1	13
	H3f3a right arm		5.5				7.5
	H3f3b right arm		4.8				8.2
pcDNA 3.1+ (NotI/KpnI cut)	Control	3.6	n/a				13.4
	H3f3a left arm		4.5				8.9
pcDNA 3.1+ (BamHI/KpnI cut)	Control	3.2	n/a				13.8
	H3f3b left arm		4				9.8
pcDNA 3.1+ H3f3a left arm (NotI/XhoI cut)	Control	3	n/a				14
	GFP		6				8
pcDNA 3.1+ H3f3b left arm (BamHI/XhoI cut)	Control	3.4	n/a				13.6
	RFP		5.2				8.4
pIndu H3f3a right arm (HindIII/BamHI cut)	Control	3	n/a				14
	H3f3a left arm-GFP + ERT2		4.2	5			4.8
pIndu H3f3b right arm (KpnI/BamHI cut)	Control	3.5	n/a	n/a			13.5
	H3f3b left arm-RFP + ERT2		3.8	5			4.7

p-eGFP-N1 (EcoRI/BamHI cut)	Control	4.4	n/a	n/a			12.6
	H3.3		10				2.6
	H3.3K27M		6.2				6.4
RCAS (ClaI/NotI cut)	Control	4	n/a				13
	H3.3-GFP loxp		4.3				8.7
	K27M-GFP loxp		5				8

Table 3.16. Reaction volumes for ligations.

3.15. Agarose Gel Electrophoresis

1% agarose gels were prepared by adding 1.5 mg of agarose to 150 ml 1x TAE buffer. 15 µl of 10000X GelRed stock solution was added. After the gel polymerized, the wells were loaded with a variable amount of PCR product depending of the application. 5 µl of MassRuler Express Reverse DNA Ladder Mix (SM1293) was used as a marker.

3.16. Agarose Gel Extraction

Agarose gel extraction was done using the QiaQuick Gel Extraction Kit according to the manufacturer's protocol.

3.17. BAC purification

H3f3a and H3f3b BAC clones (Clones RP24-252A14 and RP24-205P9 respectively) were received from the BACPAC Resource Center of the Children's Hospital Oakland Research Institute (CHORI) as stab-cultures in LB agar containing 12.5 µg/ml chloramphenicol. The stab was gently scratched using a sterile pipette tip and transferred to a sterile 1.5 ml tube containing 1ml of LB medium. Serial dilutions of 10^{-3}, 10^{-5} and 10^{-7} of the BAC clone-harboring bacteria were made and the dilutions were inoculated in LB agar plates containing 25 µg/ml chloramphenicol. Plates were then incubated at 37°C overnight.

Single colonies were picked and inoculated in 5 ml overnight cultures overnight at 37°C with shaking. 1 ml of each culture was kept to establish a glycerol stock in case a clone is selected.

The remaining 4 ml of the culture was sequentially centrifuged into a 1.5 ml tube for 5 min at 10000g. Supernatants were discarded and LB traces were carefully removed after the last centrifugation to add 300 ml of Qiagen buffer P1. Bacteria were resuspended by gentle pipetting. 300 ml of Qiagen buffer P2 was added and mixed 6-8 times by inverting the tube and later incubated at room temperature for 5 min. Finally, 300 ml of Qiagen buffer P3 was added and the tubes were mixed by inverting. Tubes were then incubated on ice for 5 min and later spun for 10 min at 10000g at 4°C.

800 ml of the supernatant was transferred to a new tube. BAC DNA was precipitated by adding 540 ml of isopropanol and mixed gently by inverting the tube. DNA samples were then spun for 10 min at 10000g at 4°C. Supernatant was discarded and 500 ml of 70% (v/v) ethanol was added to wash the pellet prior to another centrifugation for 5 min at 10.000g at 4°C. Supernatant was removed again and samples were spun shortly at room temperature before removing all traces of supernatant. Tubes were left open for 2-3 min to allow the pellets to dry. BAC DNA samples were dissolved in 40 ml TE pH 8.0 and, due to the difficulty of dissolving a BAC compared to a plasmid, the tubes were incubated at 4°C for 2 hours and mixed by tipping occasionally. Later the isolated BAC DNA samples were stored at 4°C.

3.18. Preparation of competent cells for electroporation

Serial dilutions of 10^{-3}, 10^{-5} and 10^{-7} of the SW105 bacterial cells were prepared and plated on LB agar plates without antibiotics. Agar plates were incubated for 20 h at 32°C. Single colonies from each plate were inoculated into 5 ml LB culture and incubated overnight at 32°C.

During the preparation of electroporation-competent bacteria conditions were kept as close to 0°C as possible. Glass pipettes were pre-cooled by pipetting a 0°C cold solution prior to pipetting the bacteria and the bacteria were kept on ice. Competent bacteria for

electroporation were prepared freshly right before electroporation. Next morning 3 h before its use 500 ml sterile 10% (v/v) glycerol in H_2O was cooled on ice. 2 ml of the overnight cultures were transferred to Erlenmeyer flasks containing 50 ml of LB medium and grow for 3-5 hours. Absorbance at 600 nm was measured after 3 hours until cultures reached 0.45-0.5. After cultures reached an absorbance of 0.5, they were transferred to pre-cooled 50-ml Falcon tubes and spun down at 4000g for 10 min at 0°C in a pre-cooled rotor. Supernatants were discarded and the tubes were inverted on a stack of tissue paper at 4°C to dry the remaining supernatant.

Tubes were put back on ice and 50 ml of ice-cold 10% (v/v) glycerol was added to resuspend the cells. Samples were centrifuged at 4000g for 10 min at 0°C and two more steps of 10% glycerol were performed. After the last wash, supernatant was removed; save for 0.7 ml, which was then aliquoted into pre-cooled 1.5 ml tubes with 50 µl/tube. These aliquots were used immediately for electroporation.

3.19. BAC electroporation into competent cells

100 µl electroporation cuvettes were placed on ice 5 min prior to use. Tubes containing aliquots of competent bacteria as well as purified BAC samples (H3f3a and H3f3b BACs) were also placed on ice. The electroporations were prepared by pipetting 50 µl of the competent bacteria and 1 µl of the purified BAC into the cuvette. The cuvette was placed in the electroporation device (BioRAD Gene Pulser) and a pulse was delivered at 2.3 kV with 25 µF and the pulse controller was set to 200 Ω. Following the pulse, 1 ml of LB medium was added to the cuvette and then the whole volume was transferred to a 1.5 ml centrifuge tube. Two additional electroporations were performed for each BAC using 2 µl and 5 µl of the purified BAC.

All tubes containing electroporated bacteria in LB were incubated for 1 h at 32°C with shaking. Two plates from each electroporation were made, one containing 10% of the culture volume and another containing the remaining. LB agar plates containing 25 µg/ml chloramphenicol were incubated for 20 h at 32°C.

3.20. Preparation of competent cells for homologous recombination

The same procedure for the preparation of competent cells for electroporation was used with the following modifications: when the cells reached an absorbance of 0.5 at 600 nm the culture was transferred to a shaking water bath at 42°C for 15 min to induce the bacterial recombinase activity. After the incubation, the flask with the bacterial culture was moved to an ice-slurry and shook gently until cooled down to 0°C. Then the culture was incubated for 20 min on ice. All further steps were done following the previous protocol.

3.21. Removal of the antibiotic resistance gene

To remove the antibiotic resistance gene overnight cultures of each validated and recombined BAC clones (H3f3a-GFP-ERT2 and H3f3b-RFP-ERT2 BAC) were made in LB containing 25 µg/ml chloramphenicol. Next morning 50 ml of LB (25 µg/ml chloramphenicol) was inoculated with 1 ml of the overnight culture. Cells were incubated at 32°C with shaking until they reached an absorbance of 0.5 at 600 nm. Then 0.5 ml of 10% (w/v) L-Arabinose was added. The bacterial culture was then incubated for an additional hour and diluted by taking 5 ml and adding it into a new flask with 50 ml of LB supplemented with 25 µg/ml chloramphenicol. Another incubation of the diluted cultures was done at 32°C for one hour before preparing serial dilutions (10^{-3}, 10^{-5} and 10^{-7}) and plating them on LB agar plates containing 25 µg/ml chloramphenicol. Plates were incubated for 20 h at 32°C.

3.22. Purification of H3f3b-RFP-ERT2 BAC fragment for injection using a sepharose column

H3f3b-RFP-ERT2 BAC was purified using a Sepharose CL-4B column. To prepare the sepharose column 20 ml of Sepharose CL-4B was poured into a 250 ml beaker. 150 ml of injection buffer was added to the beaker and mixed gently by swirling. Afterwards the gel was allowed to settle completely. The solution was decanted and another 150 ml of injection buffer was added. This step was repeated three more times for a total of 4 washes with the injection buffer. After the washes, sepharose was resuspended in 100 ml of injection buffer and transferred to a vessel that allowed for degassing of the gel. To degas the gel, the vessel was connected to a pump for 15 min, swirling occasionally. Then, the degassed gel was transferred to a beaker.

To prepare the column, a 5 ml Falcon serological pipette was used. Most of the cotton bud was removed and the remaining was pushed to the tip of the pipette to prevent the gel from flowing out. The column was firmly attached to a holder in a vertical position. The bottom part of the column was closed using a pipette tip with parafilm wrapped around it. The column was filled with injection buffer up to two-thirds of its height. The beaker with the gel was swirled gently to resuspend the sepharose and then the gel was applied with a Pasteur pipette to the column filling it up to the top. Once 1 cm of the gel matrix was settled down the outflow was open and the eluate was collected in a beaker. Gel was continuously applied down the column until the gel reached 2-3 cm from the top of the column. After the packing was finished a 50 ml syringe without the piston was connected to the top of the column using parafilm and filled with injection buffer. The column was washed with 30 ml of injection buffer and then the 50 ml syringe was removed. When there was almost no buffer left on top of the gel, the BAC sample (100 µl) was applied. The solution was allowed to

enter the gel and then an additional 100 µl of injection buffer was applied. After the buffer entered the column another 100 µl of injection buffer was applied to the top of the column and allowed to enter. After this second round of 100 µl the column was filled with injection buffer, the 50 ml syringe was reattached and filled with injection buffer. 300 µl fractions were collected until 40-50 fractions left the column and then the column was stopped. The absorbance at 260 nm was measured for every fraction to identify the fractions containing the BAC fragments.

3.23. Purification of H3f3a-GFP-ERT2 BAC fragment for injection by nucleic acid extraction, concentration and dialysis

To purify the H3f3a-GFP-ERT2 BAC fragment the corresponding 110 kb band was excised from the agarose gel after running a PFGE. The agarose block was then put inside a Maxi D-tube dialyzer and placed into an electrophoresis chamber filled with 0.5X TAE buffer. Following the manufacturer protocol, an elution time of 90 min at 100 V was used. After eluting the DNA fragment into the TAE buffer, the sample was concentrated using Microcon Centrifugal Filter columns to a final volume of 100 µl, following the standard protocol provided by the manufacturer. The final 100 µl was then pipetted on top of a Millipore Membrane floating in a petri dish with 100 ml injection buffer and dialyzed for 3 hours at 4°C.

3.24. Pulse Field Gel Electrophoresis

1% agarose gels were prepared by adding agarose (for PFGE) to 0.5X TAE buffer. After the gel polymerized, a piece of a block of the precast ladder (CHEF DNA Size Standard Lambda Ladder) was cut and embedded into the first well using some of the agarose previously melted. After the marker was casted into the gel, the PFGE was run using a CHEF-DR III

System from BioRad according to the manufacturer's protocol with the following settings: 6 V/cm, pulse angle 120, initial switching time 0.5 sec, final switching time 20 sec, run time 14 h and cooling set to 14°C. Later, the PFGE gels were post-stained with Ethidium Bromide (1mg/ml solution) when necessary.

3.25. Bacterial transformation

Bacterial transformation was done using DH5α E.coli strain. For each reaction, 50 µl of DH5α cells was thawed on ice. After thawing, 10 µl of the ligation reaction was added to the 50 µl of cells, and the solution was mixed and incubated on ice for 30 minutes. The mixture of cells and ligation reaction was then heat-shocked for 90 seconds at 42°C to permeabilize the cells. After the heat shock, cells were incubated for 2 minutes on ice. 1 ml of LB medium was added to each of the samples and they were left shaking for 1 hour at 37°C before being centrifuged at 6000 r.p.m. and the resuspension of the pellet in 200 µl LB medium. The resuspended bacteria were then spread into ampicillin agar plates and incubated overnight at 37°C.

3.26. Colony Miniprep

5 colonies from each transformation group were picked and inoculated into 5 ml LB medium with ampicillin. These cultures were incubated overnight shaking at 37°C and miniprep was performed according to manufacturer's protocol using QiaPrep mini prep Kit (27106).

3.27. Genotyping

Genomic DNA was isolated from tail tip biopsies using NID buffer plus 1% Protein-kinase K and incubating at 56 degrees for three hours. Genotyping of the BAC mouse lines was done from tail and/or ear biopsies. Genotyping was performed by PCR following the protocol described in **Section 3.12** (**Table 3.12**).

3.28. DF-1 cell culture and transfection

DF-1 chicken cells were used for the production of the different RCAS viruses. They were grown in DMEM (ATCC, 30-2002) supplemented with 10% FBS (ATCC, 30-2020) and 1% Penicillin/Streptomycin (Life technologies, 15140122) and incubated at 39°C in a humidified incubator with 5% CO2. For the transfection of the RCAS constructs a vial of early passage DF-1 cells was thawed, expanded and split into cell culture flasks (Greiner bio-one, 690175) such that the cells will reach a confluence of 60% on the day of the transfection. To perform the transfection, 4 µg of plasmid and 10 µl of FugeneHD (Promega, E231A) were diluted in 200 µl of Opti-MEM and incubated at room temperature for 15 min. After the incubation, the mixture was directly added to the flask containing DF-1 cells. Medium was changed 12 h after the transfection and every transfection was checked after 3-5 days under the microscope using RCAS-GFP plasmid as a positive control. Transfected cells were used for injection into pups 7-14 days post-transfection.

3.29. Primary brain tumor induction

To induce primary brain tumors in our mouse model, DF-1 cells were transfected with the following constructs: RCAS-AKT, RCAS-PDGFB, RCAS-luciferase, RCAS-GFP, RCAS-H3.3-GFP and RCAS-H3.3K27M-GFP. On the day of injection, single cell suspensions of each of the cultures were prepared and the concentration was measured. DF-1 cells expressing each of the constructs were combined as shown in Table ? and the final concentration of each cell type was adjusted to $4x10^4$ cells/µl.

Group	Combination
GFP	RCAS-GFP + RCAS-AKT + RCAS-PDGFB + RCAS-luciferase
H3.3	RCAS-H3.3-GFP + RCAS-AKT + RCAS-PDGFB + RCAS-luciferase
K27M	RCAS-H3.3K27M-GFP + RCAS-AKT + RCAS-PDGFB + RCAS-luciferase

Table 3.17. Combination of RCAS constructs injection.

1 µl of the cell mixture was injected into one of two different locations in the brains of neonatal Nestin-TVA or Nestin-TVA/Nestin creERT2 animals by an intracranial injection using a 10 µl Hamilton syringe. First location was the SubVentricular Zone (SVZ) of the hippocampus of the right brain hemisphere (red arrow, **Figure 3.1**) and the second one was the pons (blue arrow, **Figure 3.2**). The coordinates for the intracranial injection in the first case were 1/3 of the distance between Bregma and Lambda and 1.5 mm depth. For the pons injection, coordinates were 1 mm posterior to Lambda and 3 mm depth.

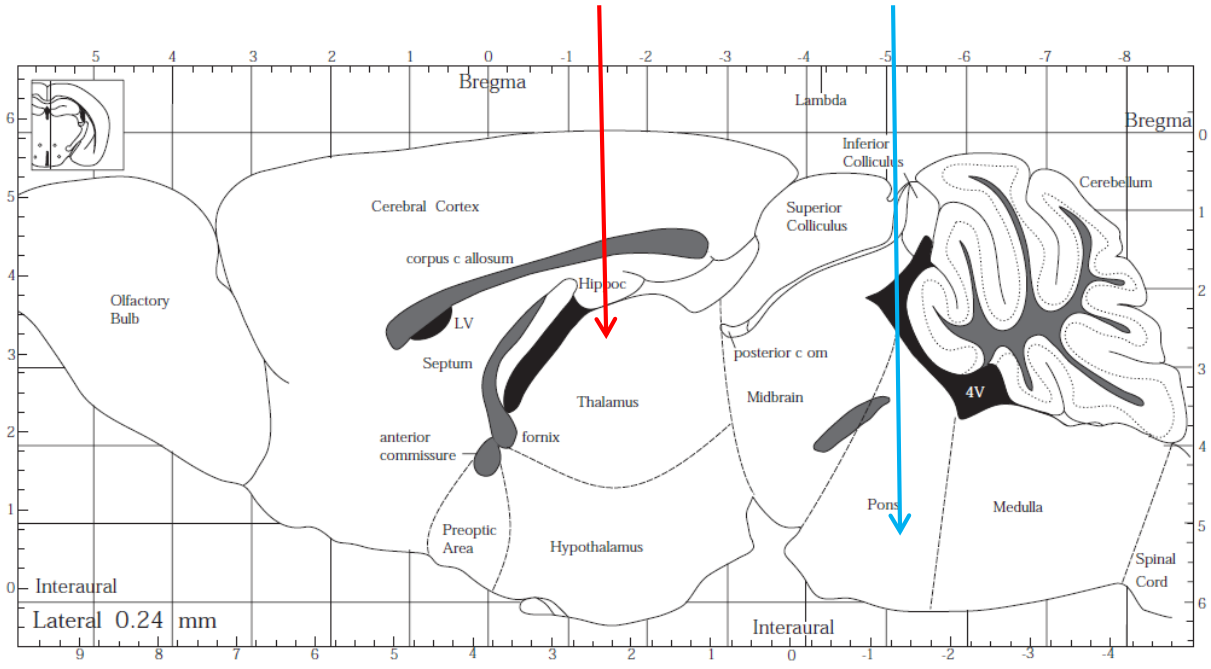

Figure 3.1. Schematic representation of a sagittal cut of the mouse brain showing the location of the intracranial injections.

3.30. Bioluminescence Imaging

Detection and monitoring of tumor growth was done by Bioluminescence Imaging (BLI), using IVIS Lumina II In Vivo Imaging System (Perkin Elmer). Owing to the fact that our tumor model includes the injection of RCAS-luciferase into the mouse brain, tumor cells express the luciferase enzyme. This enzyme, in the presence of O_2, converts the substrate D-luciferin into oxyluciferin and produces light. Animals were given an injection of D-luciferin (Biocat, 7903-1g-BV) intraperitoneally. D-luciferin was dissolved in PBS and the final concentration

administered was 150 mg/Kg of body weight. Following the injection, animals were anesthetized using the XGI-8 system provided with the IVIS and imaged by taking 1 picture every minute for at least 20 min. The parameters were: exposure time: 1 min (in the case of the signal being too high, the exposure time was reduced to 30 sec, 15 sec or 5 sec to avoid overexposure), high binning and aperture lens position: F1. Light was then detected by the IVIS system and displayed as a pixel image, overlapping with a photograph of the animals being imaged. A Region of Interest (ROI) was then drawn over the head of the mouse using the Living Image 4.3.1 software provided with the IVIS system and the total signal was calculated in photon/sec (p/s). A curve with the measurements of each mouse over the 20 min (or more when necessary) of imaging was plotted and the peak value was then selected as the BLI value for that day as shown in **Figure 3.2**.

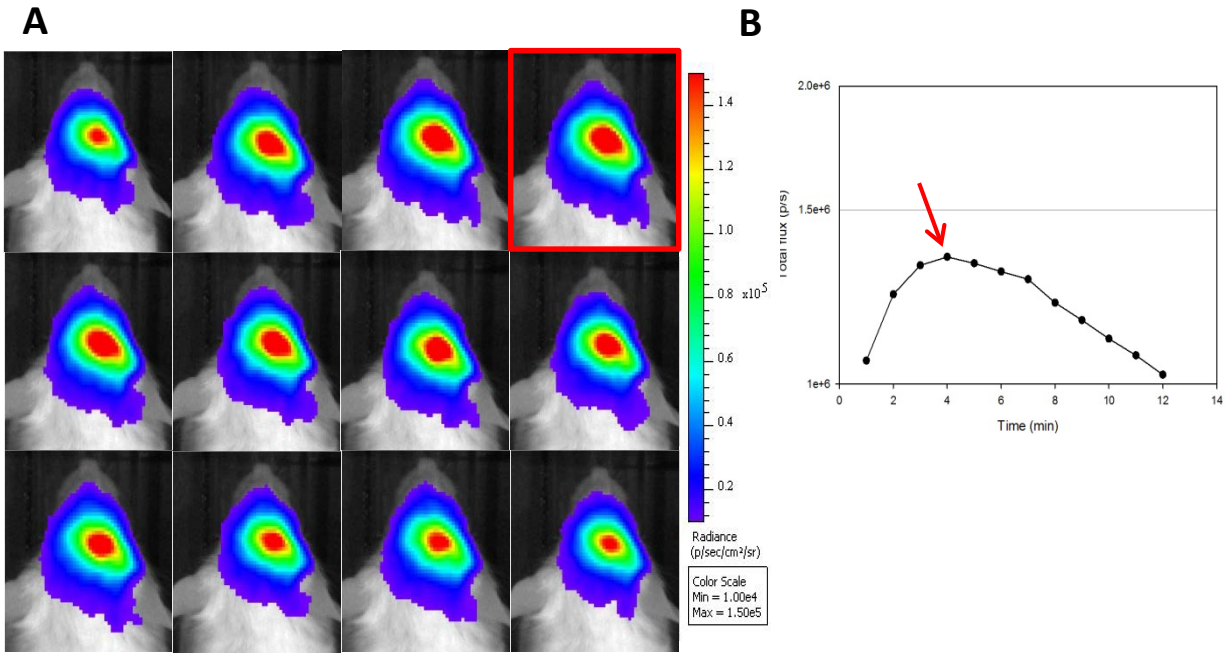

Figure 3.2. BLI measurement. (A) BLI pictures taken every minute after D-luciferin injection. **(B)** Bioluminescence (photons per second) signal over time, red arrow point at the peak of the signal.

3.31. Tumor tissue sampling

Following the criteria mentioned in **Table 3.11**, animals were sacrificed upon reaching a threshold of 20 points. Animals were euthanized using a CO_2 chamber. To extract the brain the head area was soaked with 70% Ethanol and the animal was then beheaded using strong scissors. The surface of the skull was revealed by cutting off the skin of the head using smaller scissors. The skull was cut into pieces using strategically placed incisions between the eyes and parallel to the ears until the upper part of the skull could be separated from the brain. Finally, carefully using a small spoon, the brain was removed from the rest of the skull and placed in a 15 ml Falcon tube containing 4% PFA for fixation. The brain sample was then put through the process described in **Table 3.18** for fixation and embedding of the tissue.

Solution	Time	Temperature	Comments
Fix in 4% PFA	overnight	4°C	pH 7,2
PBS	2 X 15 min	Room temperature	
70% Ethanol	2 X 30 min	Room temperature	
85% Ethanol	60 min	Room temperature	
95% Ethanol	60 min	Room temperature	
100% Ethanol	60 min	Room temperature	Change solution once
Xylol	2 X 60 min	Room temperature	
Paraffin	3 X 60 min	60°C	
Paraffin block	Indefinite	Room temperature	

Table 3.18. Fixation and paraffin embedding protocol.

3.32. Paraffin sectioning

Paraffin embedded tissues were sectioned using a microtome (Leica RM 2255). Paraffin blocks were placed into the cutting platform and excess of paraffin was removed using a blade. The paraffin block was trimmed by 50 µM sections until the tissue sample was reached. Once at the desired location, 6 µM sections were cut. After cutting 4-5 sections, these sections were transferred to a water bath at 39°C filled with distilled water and

allowed to spread. When the tissue expanded and there were no more wrinkles, the sections were taken in a slide and placed in a heat block at 39°C for further drying. When the slides were dry they were placed into slide boxes and incubated at 37°C overnight.

3.33. Haematoxylin & Eosin staining

Haematoxylin & Eosin staining of the paraffin sections was done following the protocol shown in **Table 3.19**. Haematoxylin and Eosin solutions were filtered prior to each use.

Solution	Time
Xylene	2 X 5 min
100% Ethanol	2 X 5 min
70% Ethanol	5 min
Distilled water	5 min
Haematoxylin	8 min
Distilled water	Clean shortly
Running tap water (warm)	5 min
Eosin (0.1%)	90 sec
Distilled water	Dip in
70% Ethanol	3 min
85% Ethanol	3 min
100% Ethanol	2 X 5 min
Xylene	2 X 5 min

Table 3.19. Haematoxylin & Eosin staining protocol.

3.34. Immunohistochemistry staining

Immunohistochemistry staining of the paraffin sections was done using the protocol in **Table 3.20**. Citrabuffer was prepared by diluting Concentrated Antigen Retrieval Citra Solution (Biogenex, HK086-9K) 1:10 in distilled water. H_2O_2 3% was prepared by diluting Hydrogen peroxide 30% (A1134-1000, Applichem) 1:10 in PBS/Methanol (1:1). Normal Swine Serum (NSS) was diluted in PBS. The primary antibody was diluted in 5% NSS and the secondary antibody was diluted 1:400 in 5% NSS. AB-Complex (PK-4000, Vector Laboratories) was prepared 30 min in advance and diluted 1:100 in PBS. Diaminobenzidine was prepared by dissolving 1 silver tablet and 1 gold tablet (D4293-50SET, Sigma) in 5ml of distilled water.

Day 1	
Solution	**Time**
Xylene	2 X 5 min
100% Ethanol	2 X 5 min
95% Ethanol	2 X 5 min
70% Ethanol	5 min
Distilled water	5 min
PBS	5 min
Citrabuffer	Microwave 2 min at maximum watt
	Microwave 8 min at 360 watt
	30 min cool down to room temperature
PBS	5 min
3% H_2O_2	8 min
PBS	5 min
Circle sections with PAP-Pen and put them in moist chamber	
5% NSS	30 min
Primary antibody	Overnight, 4°C
Day 2	
PBS	3 X 5 min
Secondary antibody	30 min
PBS	3 X 5 min
AB-Complex	30 min
PBS	2 X 5 min
DAB	Variable, stop reaction with water
70% Ethanol	5 min
95% Ethanol	2 X 5 min
100% Ethanol	2 X 5 min
Xylene	2 X 5 min
Mount sections using Eukitt	

Table 3.20. IHC staining protocol.

3.35. Immunofluorescence staining

Immunofluorescence staining of the paraffin sections was done following the protocol in **Table 3.21**. Citrabuffer, NSS and primary antibody were prepared as described in **Section 3.34**. Secondary antibody was diluted 1:400 in PBST.

Day 1	
Solution	**Time**
Xylene	2 X 5 min
100% Ethanol	2 X 5 min
95% Ethanol	2 X 5 min
70% Ethanol	2 X 5 min
Tap water	5 min
PBS	5 min
Citrabuffer	Microwave 2 min at maximum watt
	Microwave 8 min at 360 watt
	30 min cool down to room temperature
PBS	5 min
Circle sections with PAP-Pen and put them in moist chamber	
5% NSS	30 min
Primary antibody	Overnight, 4°C
Day 2 (Kept in the dark)	
PBST	3 X 5 min
Secondary antibody	1 h
PBST	2 X 5 min
Mount sections using Vectashield mounting medium	

Table 3.21. Immunofluorescence staining protocol.

3.36. Laser scanning microscopy imaging and image analysis

Brightfield and fluorescence pictures of the DF-1 cells in culture were taken using a Zeiss Cell Observer Microscope. Brightfield pictures of the DAB stainings were taken using a Zeiss Axiophot or a Zeiss AxioScan.Z1 microscope. Fluorescence pictures of the paraffin sections after immunofluorescence staining were taken using a Zeiss LSM 700/780/800 microscope. All processing and counting of the images were done using either Fiji or Zen (Blue edition) software.

3.37. Statistical analysis

Statistical analysis was performed using Sigma Plot version 12.5. Quantitative experiments were repeated at least three times independently and the results were presented as mean ± s.d. One-Way Analysis of Variance (ANOVA) was used to determine statistical significance among three or more groups with a post-hoc Bonferroni t-test for pairwise multiple comparison. Survival analysis was presented using a Kaplan-Meier survival curve, and the survival curves comparison was done by log-rank test.

4. Results

4.1. Establishment of a DIPG mouse model

4.1.1. Cloning of RCAS-H3.3-GFP and RCAS-H3.3K27M-GFP

In order to trace and be able to delete the histone H3.3 using our mouse tumor model we tagged H3.3 and H3.3K27M with GFP and flanked the DNA sequence with loxp sites. H3.3/H3.3K27M DNA were excised from the pBabe vector as shown in **Figure 3.1A** and cloned into the p-eGFP1-N1 which fused the C-terminus of H3.3/H3.3K27M to the GFP protein. Upstream and downstream loxp sites were added by PCR amplification of H3.3-GFP/H3.3K27M-GFP (**Figure 3.1C**) and cloned into the RCAS vector substituting the AKT insert (**Figure 3.1B**). Positive colonies were identified (**Figure 3.1D**) and sequenced to confirm the correct sequence for the vectors.

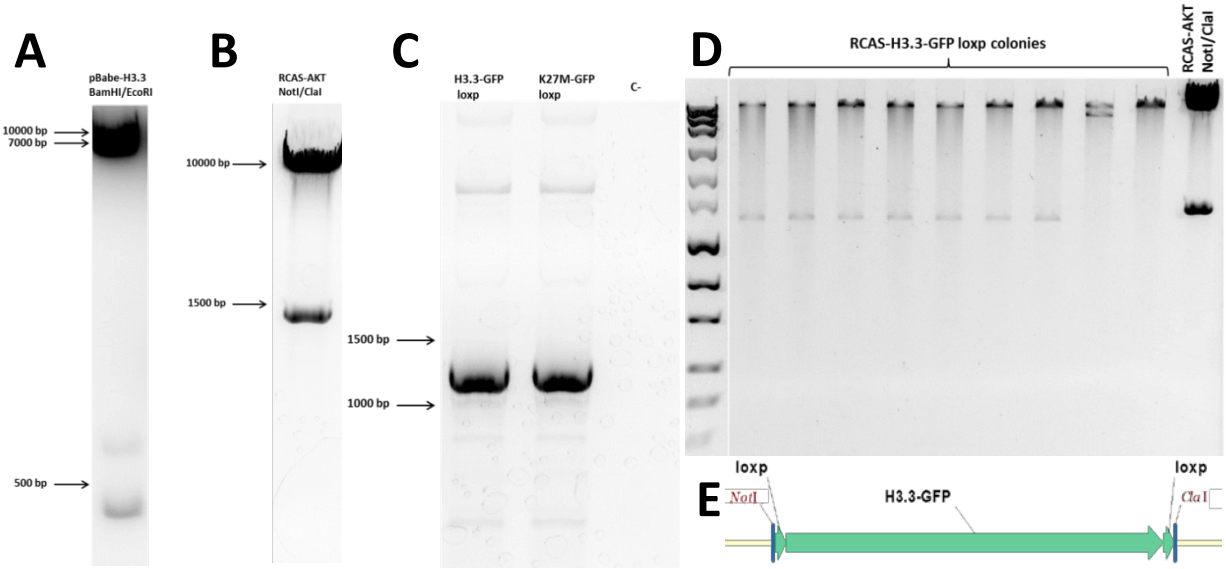

Figure 3.1. Cloning of H3.3 constructs into the RCAS vector. (A) Agarose gel electrophoresis of the pBabe-H3.3 vector after enzymatic digestion with BamHI and EcoRI. H3.3 insert can be observed as an approximately 400 bp band. **(B)** Agarose gel electrophoresis of the RCAS-AKT vector after enzymatic restriction with NotI and ClaI. **(C)** Agarose gel electrophoresis of inserts H3.3-GFP loxp and K27M-GFP loxp after PCR amplification. The phusion protein H3.3-GFP loxp can be seen as a 1.2 kb band. **(D)** Agarose gel electrophoresis of enzymatic restriction analysis from bacteria colonies potentially carrying RCAS-H3.3-GFP loxp or RCAS-K27M-GFP loxp. DNA was cut using ClaI and NotI, RCAS-AKT is included as a control. **(E)** Map of the insert region of the vector RCAS-H3.3-GFP loxp.

4.1.2. RCAS-H3.3-GFP and RCAS-H3.3K27M-GFP expression in DF-1 cells

In order to confirm the functionality of the RCAS-H3.3-GFP/RCAS-H3.3K27M-GFP vectors, DF-1 cells were transfected with both vectors as well as RCAS-GFP as a positive control and RCAS-AKT as a negative control. GFP expression was observed to be nuclear in RCAS-H3.3-GFP/RCAS-H3.3K27M-GFP compared with RCAS-GFP as expected (**Figure 3.2B, D and F**) and 3-5 days after transfection the totality of the cells expressed the vector (>95% of the cells).

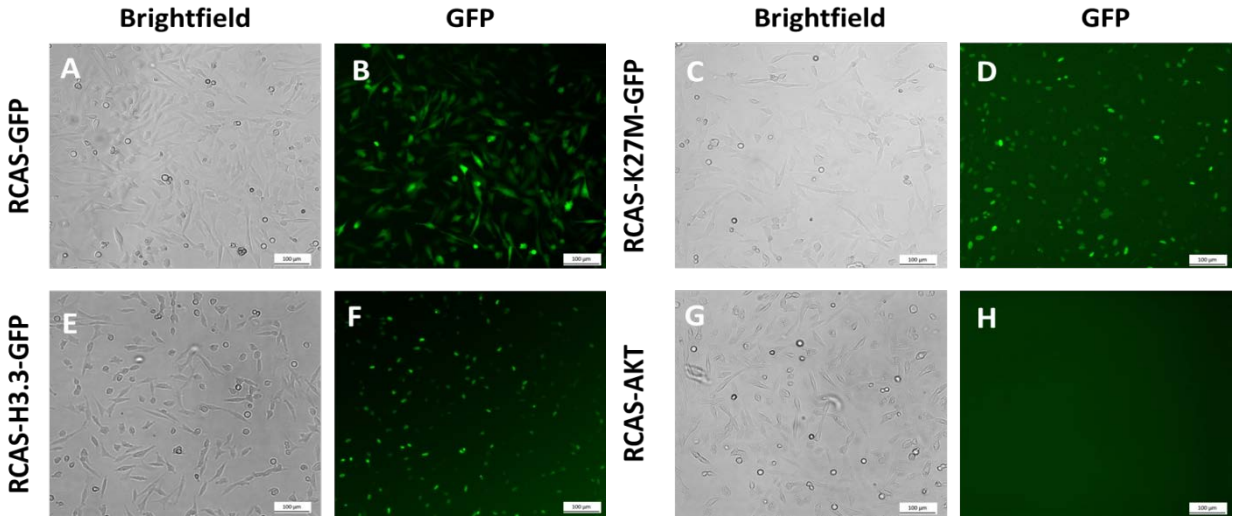

Figure 3.2. RCAS-H3.3-GFP and RCAS-K27M-GFP expression in DF-1 cells. (A, C, E and G) Brightfield images of DF-1 cells in culture expressing RCAS-GFP, RCAS-H3.3-GFP, RCAS-K27M-GFP or RCAS-AKT. **(B, D, F and H)** Representative fluorescence pictures of DF-1 cells in culture expressing RCAS-GFP, RCAS-H3.3-GFP, RCAS-K27M-GFP or RCAS-AKT.

4.1.3. In vivo tumor growth can be monitored by Bioluminescence Imaging

In order to monitor tumor growth in our tumor model, RCAS-luciferase was delivered into the SVZ of the mouse brain in combination with the other oncogenes. As shown in **Figure 3.3**, light emission (photons per second) from the tumor cells carrying the luciferase enzyme was detected with the help of IVIS Lumina II device. Biweekly imaging of the experimental animals showed the expansion of the tumor over time (**Figure 3.3A and B**)

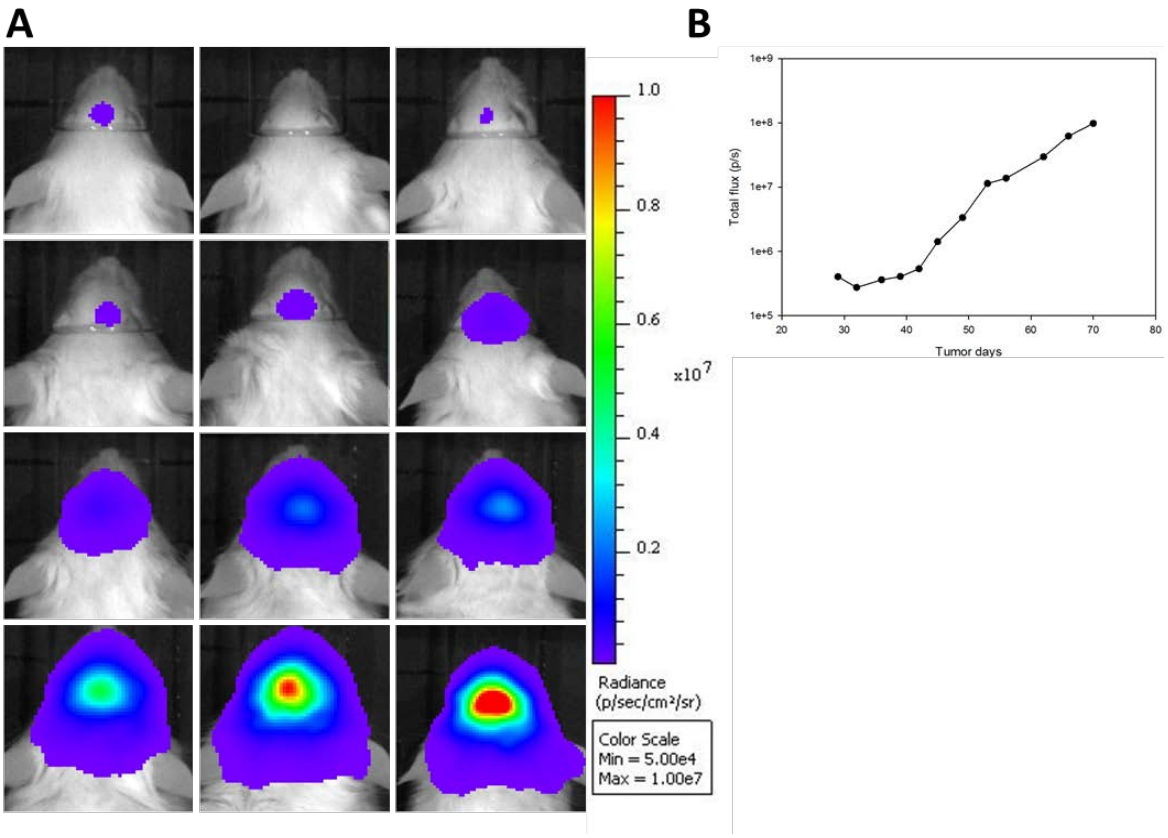

Figure 3.3. Representative BLI of a tumor. (A) BLI pictures showing tumor growth over time. **(B)** Bioluminescence measurements represented as total flux against tumor days (photons/second).

4.1.4. A High Grade Glioma model overexpressing H3.3

Histology analysis of the tumors concluded that tumors resembled HGG and displayed key features present in HGG like pseudopalisading necrosis (blue arrows in **Figure 3.4A**, **Figure 3.4C**) and active angiogenesis (red arrows in **Figure 3.4A**, **Figure 3.4B**). In addition, tumor region showed positive GFP staining indicating the expression of either H3.3-GFP or H3.3K27M-GFP.

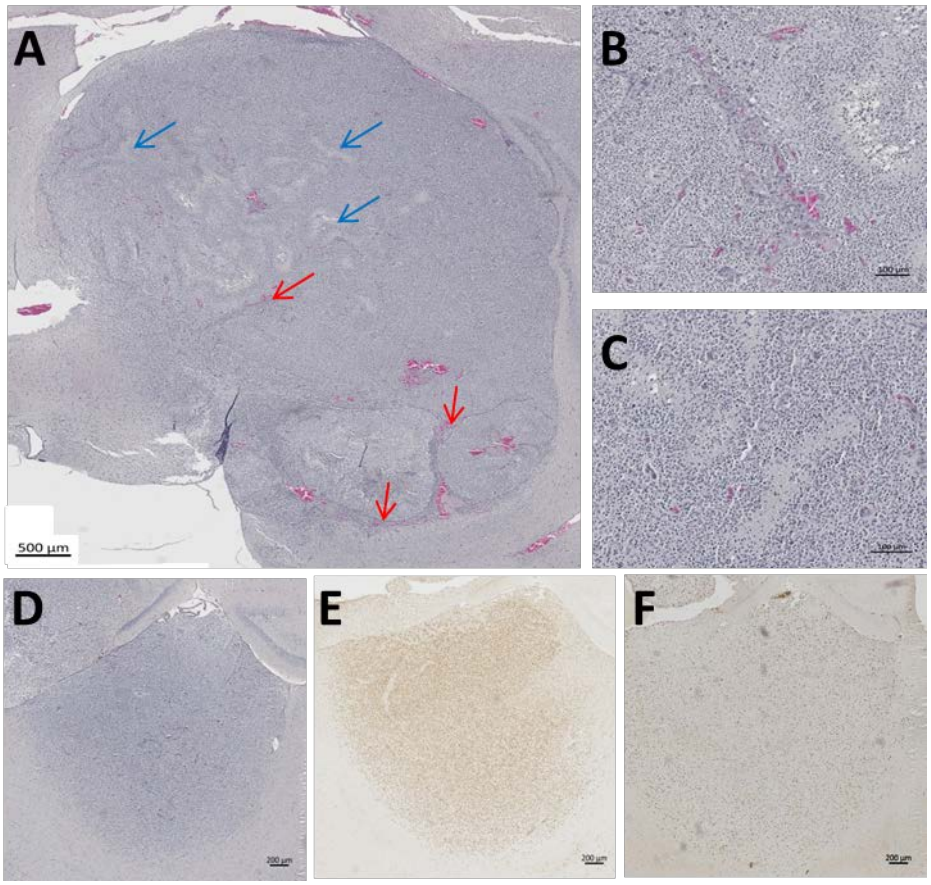

Figure 3.4. Histological features of High Grade Glioma model and marker expression. (A) Representative H&E staining of mouse tumor. Blue arrows indicate pseudopalisading necrosis and red arrows indicate angiogenesis. **(B)** High magnification picture showing the vascularization present in the tumor. **(C)** High magnification picture of pseudopalisading cells surrounding a necrotic region. **(D, E and F)** Representative pictures of the same tumor region. **D** shows H&E staining while **E** and **F** show GFP and ki67 IHC staining respectively.

A small subset of the tumors showed different tumor compartments with and without GFP expression (**Figure 3.5A** and **B**). In addition, the majority of the tumors showed regions with a mixture of GFP and non-GFP cells (**Figures 3.8L**, **3.9A** and **B**, **C** and **D**, **E** and **F**, **I** and **J**).

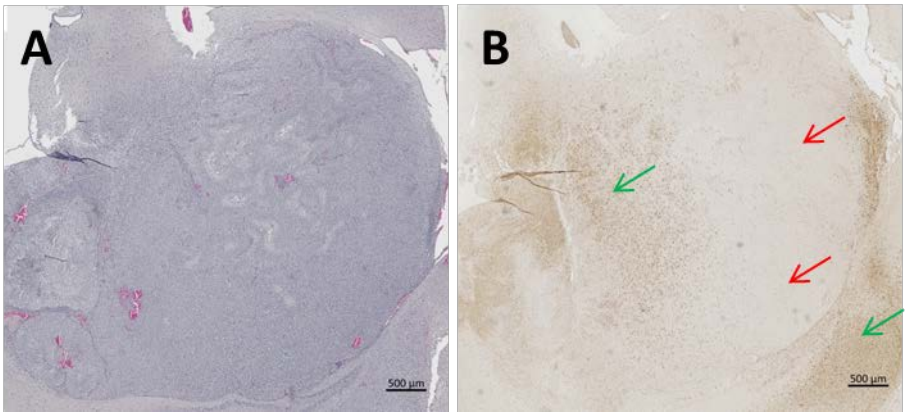

Figure 3.5. Tumor shows different compartments according to GFP expression. (A) H&E staining of a tumor induced by the over-expression of RCAS-AKT, RCAS-PDGFB and RCAS-GFP. **(B)** GFP IHC staining of the same tumor region showed in **A**. Green arrows indicate the tumor compartments which show GFP expression while the red arrows indicate the region of the tumor without GFP expression.

Since DIPGs are mainly found in the pons, we tested whether we can utilize our mouse model to induce tumors in the pons instead of the SVZ by changing the location of the injection. As shown in **Figure 3.6A** and **B**, specific targeting of the pons by intracranial injection was achieved. However, these injections did not result in HGGs. The majority of the experimental animals showed different degrees of hydrocephaly (blue arrow, **Figure 3.6C**), large blood clots in the region between the pons and the cerebellum (red arrow in **Figure 3.6C**, **Figure 3.6D**) and small tumor regions that made difficult a histological analysis of the tumors (**Figure 3.6E**). These findings suggest that the tumors provoke an early blockage of the cerebrospinal fluid (CSF) resulting in the death of the animals before tumors could be fully developed.

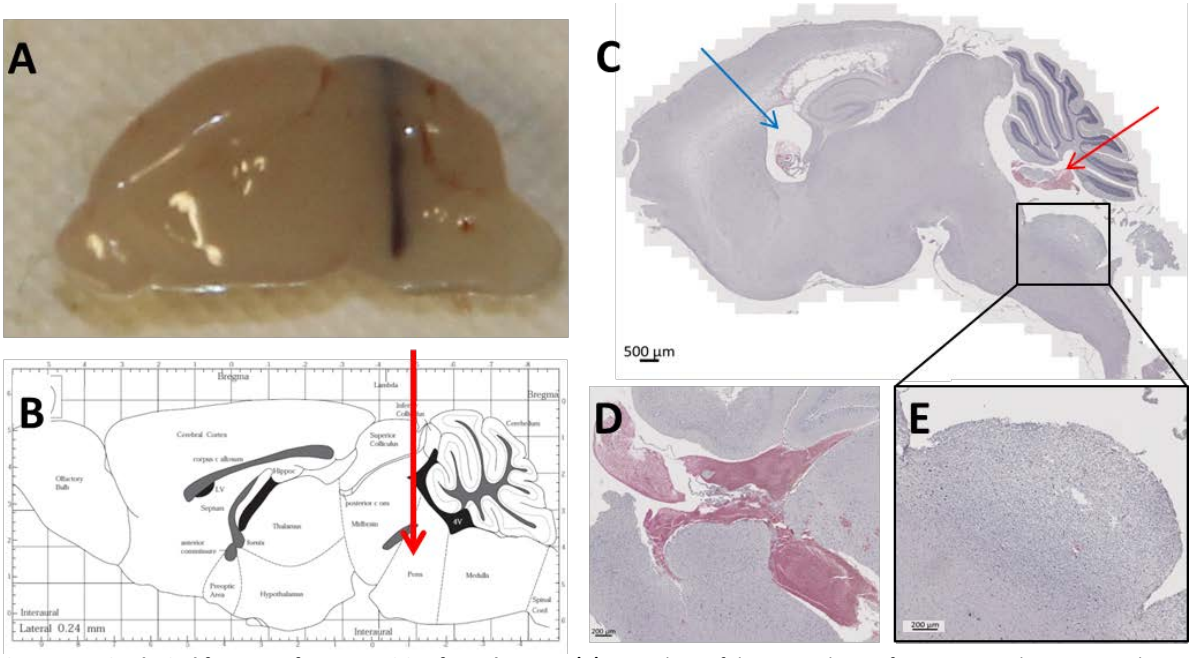

Figure 3.6. Histological features of tumors arising from the pons. (A) Sagittal cut of the mouse brain after intracranial injection in the pons with blue ink. **(B)** Sagittal schematic view of the mouse brain, red arrow indicates the location of the intracranial injection in the pons. **(C)** H&E staining of a sagittal paraffin section. Blue arrow indicates hydrocephaly and red arrow indicates a blood clot. **(D)** Representative H&E picture showing a blood clot at the same region as red arrow in **C**. **(E)** Higher magnification picture showing the tumor region abode the pons.

4.1.5. H3.3K27M over-expression reduces H3K27me3 levels

Immunohistochemistry (IHC) analysis of the H3K27me3 expression in our model showed that tumors over-expressing H3.3K27M-GFP had lower levels of H3K27me3 (**Figure 3.7**). A comparison of the H3K27me3 pattern can be seen in **Figure 3.7**, showing similar staining levels for all the groups in the cortex region, which is used as a control (**Figure 3.7D**, **E** and **F**). In contrast, K27M expressing tumors (K27M group) showed depleted H3K27me3 levels in the tumor region when compared with both control groups, GFP and H3.3 (**Figure 3.7A**, **B** and **C**).

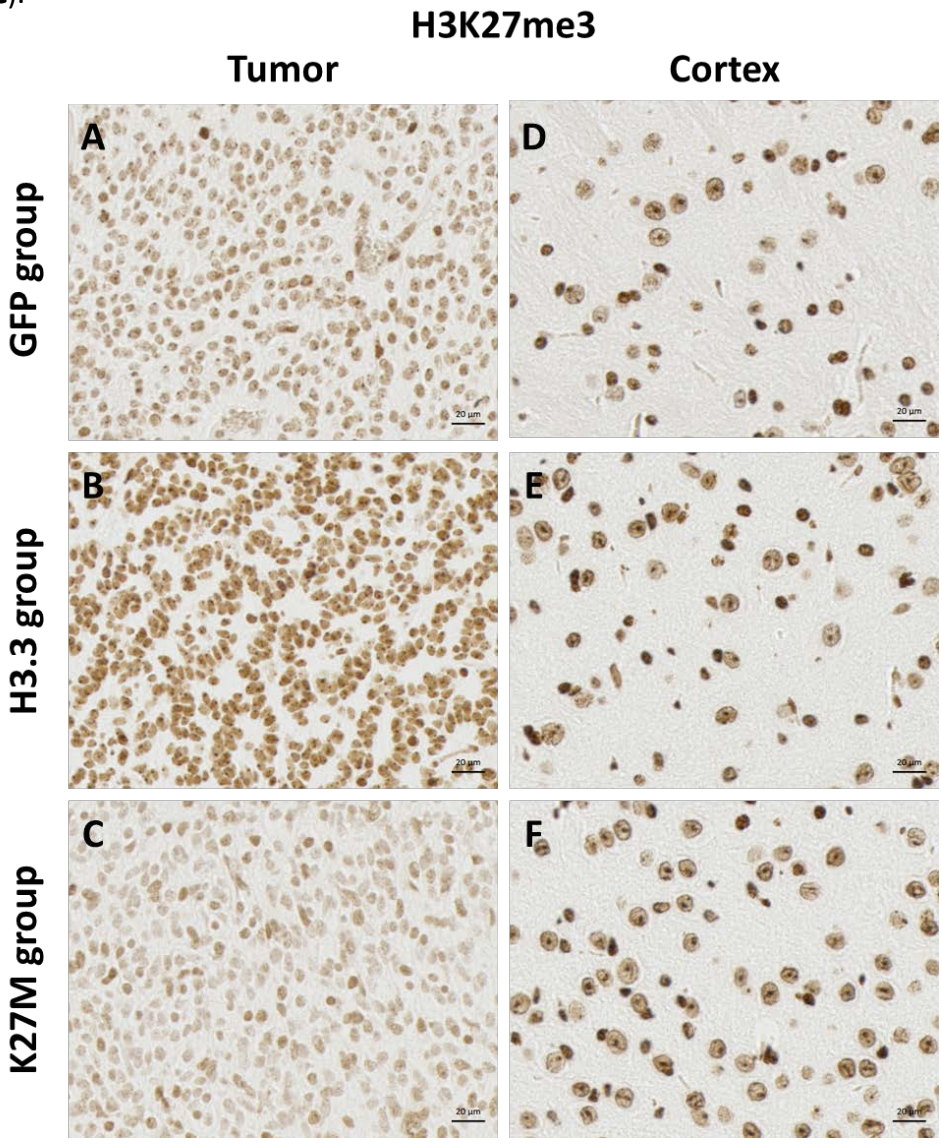

Figure 3.7. K27M-expressing tumors show reduced H3K27me3 compared to control tumors. (A-C) H3K27me3 IHC staining of the tumor region of tumors from GFP, H3.3 and K27M group. **(D-F)** H3K27me3 IHC staining of the cortex of the same brains as in **A-C**.

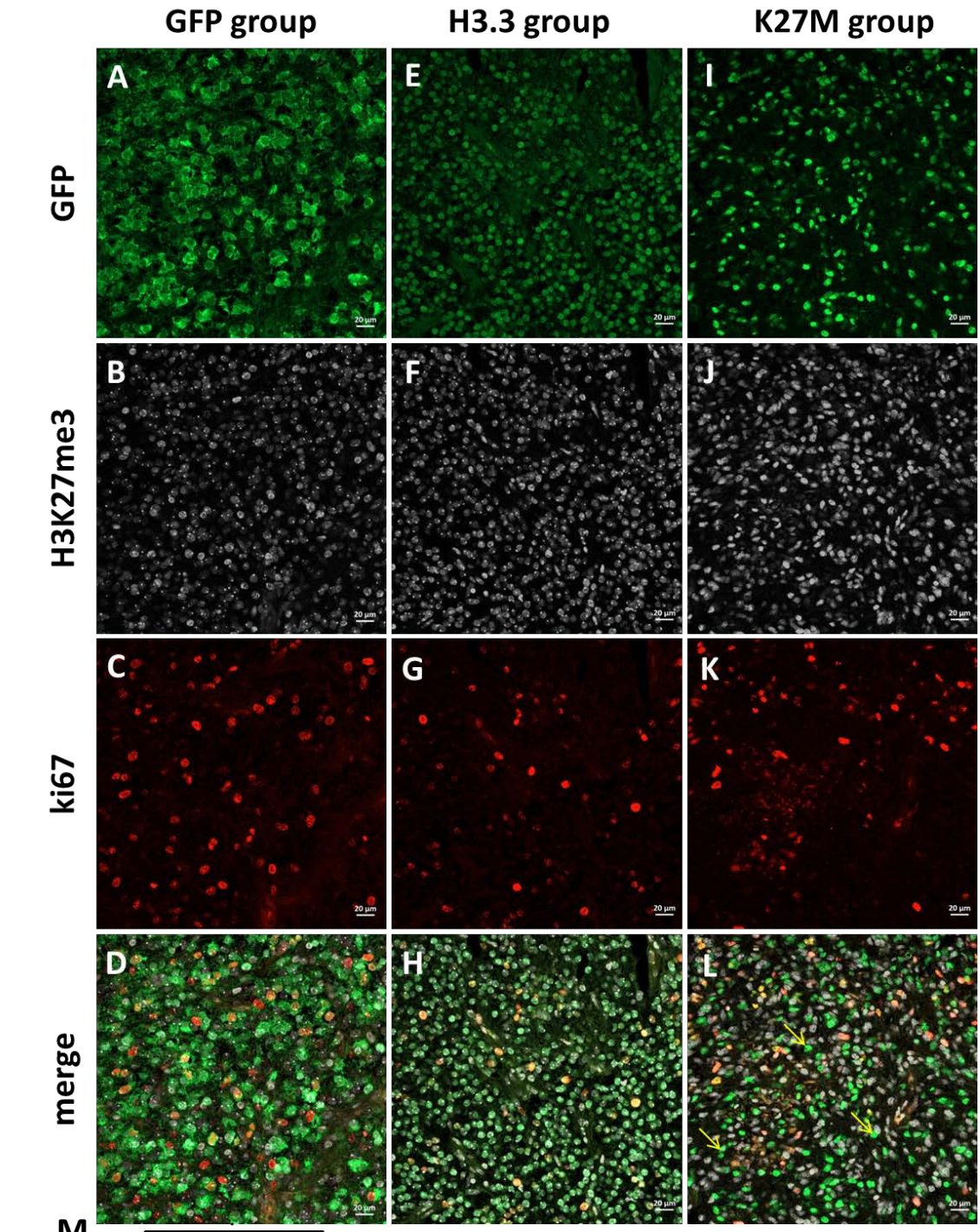

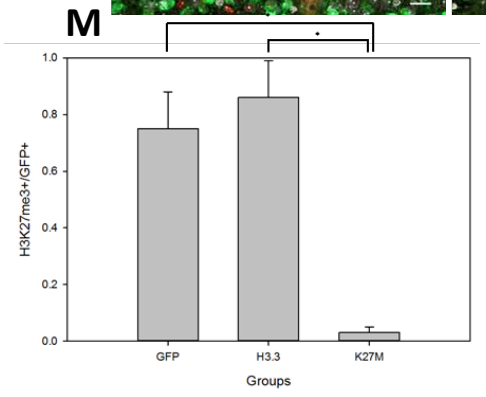

Figure 3.8. Only cells expressing K27M-GFP lose the H3K27me3. (A, E and I) GFP IF staining of tumors from the GFP, H3.3 and K27M group. **(B, F and J)** H3K27me3 IF staining of tumors from the GFP, H3.3 and K27M group. **(C, G and K)** ki67 IF staining of tumors from the GFP, H3.3 and K27M group. **(D, H and L)** Merge IF picture of tumors from the GFP, H3.3 and K27M group. Yellow arrows in **L** indicate examples of K27M-GFP expressing cells that do not show H3K27me3 expression. **(M)** H3K27me3+/GFP+ comparison between groups. One-Way Analysis of Variance (ANOVA) was used to determine statistical significance. GFP vs K27M, $p<0.002$; H3.3 vs K27M, $p<0.001$.

Immunofluorescence staining for GFP and H3K27me3 were done to analyze the co-labeling of these two markers. For the GFP and H3.3 group, most of the GFP+ cells were double positive for GFP and H3K27me3 (**Figure 3.8D**, **H** and **M**) while the K27M group showed significantly (GFP vs K27M, $p<0.002$; H3.3 vs K27M, $p<0.001$) less amount with almost no double positive cells in its GFP+ population (<5%, **Figure 3.8L** and **M**).

4.1.6. H3.3K27M deletion rescues normal H3K27me3 levels

To analyze the effect of the H3.3K27M deletion in developed tumors, NestinTVA/Nestin creERT2 animals were injected with tamoxifen 28 days after tumor induction to induce the loxp sites recombination. Upon tamoxifen injection, H3.3-GFP/H3.3K27M-GFP were deleted in the recombinase cre + animals which was confirmed by the loss of GFP expression (**Figure 3.9G** and **K**). GFP expression was unaffected in the cre - animals for H3.3 and K27M groups as well as for all animals in the GFP group (**Figure 3.9A**, **C**, **E** and **I**). Tamoxifen injection did not affect the significant (GFP cre- vs K27M cre-, $p<0.001$; H3.3 cre- vs K27M cre-, $p<0.001$) difference in H3K27me3 levels existing between K27M and the control groups in the cre- animals (**Figure 3.9A** and **B**, **E** and **F**, **I** and **J** and **M**). Comparison of co-labeling of GFP+ and H3K27me3+ cells between cre+ and cre- animals was not possible because cre+ animals from the H3.3-GFP/H3.3K27M-GFP groups did not have GFP expression. Ratio of H3K27me3+ cells from total cells was used instead to compare all the groups showing a significant difference for K27M cre- group with every other group (K27M cre- vs every group, $p<0.001$; **Figure 3.9N**). K27M cre+ group showed significantly higher H3K27me3 levels than K27M cre- group and no difference when compared with the control groups indicating that K27M deletion rescued H3K27me3 phenotype.

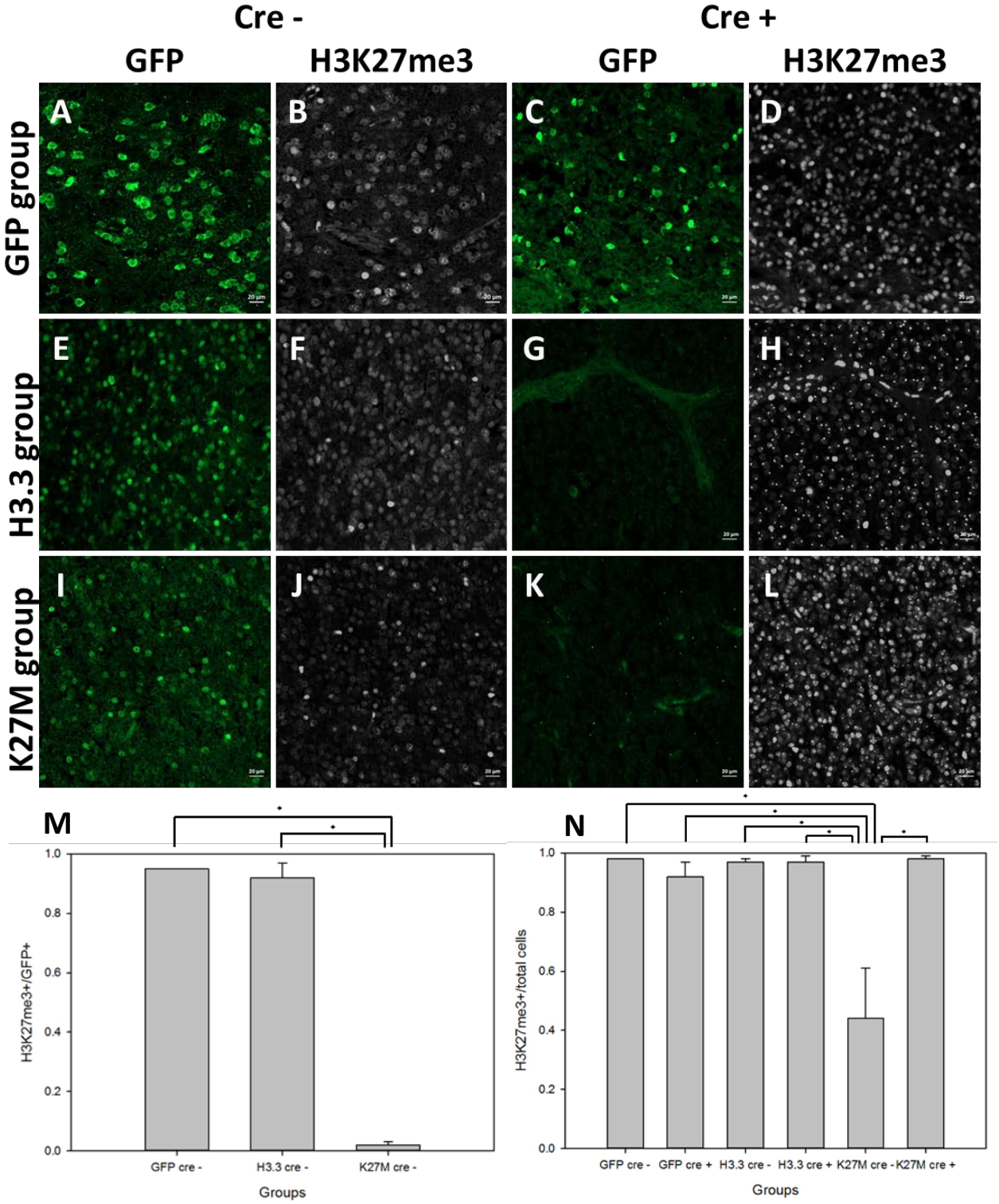

Figure 3.9. Deletion of K27M-GFP rescues H3K27me3 levels. (A, E and I) GFP IF staining of cre- animals from the GFP, H3.3 and K27M group. **(C, G and K)** GFP IF staining of cre+ animals from the GFP, H3.3 and K27M group. **(B, F and J)** H3K27me3 IF staining of cre- animals from the GFP, H3.3 and K27M group. **(D, H and L)** H3K27me3 IF staining of cre+ animals from the GFP, H3.3 and K27M group. **(M)** H3K27me3+/GFP+ comparison between groups. One-Way ANOVA was used to determine statistical significance. GFP vs K27M, $p<0.001$; H3.3 vs K27M, $p<0.001$. **(N)** H3K27me3+/total cells comparison between groups. One-Way ANOVA was used to determine statistical

significance. GFP cre- vs K27M cre-, p<0.001; GFP cre+ vs K27M cre-, p<0.001; H3.3 cre- vs K27M cre-, p<0.001; H3.3 cre+ vs K27M cre-, p<0.001; K27M cre+ vs K27M cre-, p<0.001.

4.1.7. K27M over-expression and deletion do not significantly affect survival

In order to analyze the survival, animals that did not complete the 10 days tamoxifen treatment were excluded. Additionally, only the tumors that reached a threshold of $5x10^5$ p/s 28 days after tumor induction were included in the analysis. There was no significant difference in survival within the groups when comparing cre- with cre+ animals, as shown in **Figure 3.10A**, **B** and **C**. Kaplan-Meier curves for GFP, H3.3 and K27M cre- groups did not shown survival differences (**Figure 3.10D**).

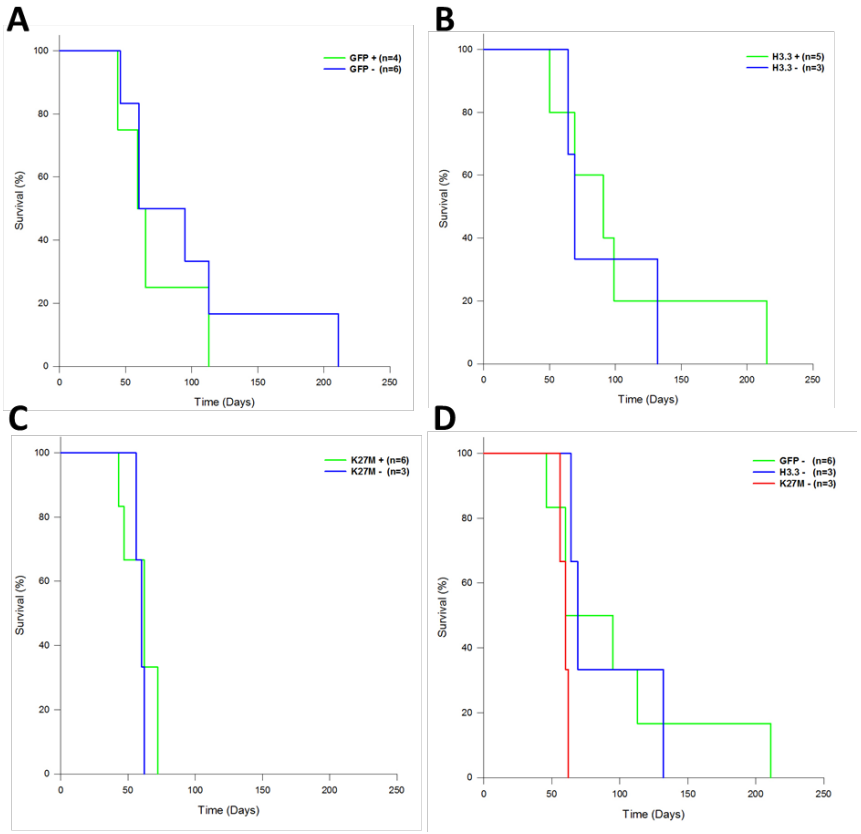

Figure 3.10. There is not significant difference in survival between K27M over-expressing and control tumors. (A) Kaplan-Meier survival analysis between GFP cre+ and cre- groups after TAM treatment. **(B)** Kaplan-Meier survival analysis between H3.3 cre+ and cre- groups after TAM treatment. **(C)** Kaplan-Meier survival analysis between K27M cre+ and cre- groups after TAM treatment. **(D)** Kaplan-Meier survival analysis between GFP, H3.3 and K27M cre- groups after TAM treatment.

4.2. Histone tracing in living behaving animals

4.2.1. pIndu H3f3a-GFP-ERT2 and H3f3b-RFP-ERT2 cloning

In order to modified the H3f3a and H3f3b BACs, the pIndu vector was modified to be used for the modification of the BACs by homologous recombination. One pIndu vector was designed to contain the fusion GFP-ERT2 with two homology arms for H3f3a while the other contained RFP-ERT2 with two homology arms for H3f3b (**Figure 3.11A**). Homology arms were designed in a way that the insertion site for GFP-ERT2/RFP-ERT2 were in the last exon of the gene sequence right before the stop codon. After recombination GFP-ERT2/RFP-ERT2 will replace the stop codon resulting in two BACs containing the sequence for the fusion proteins H3f3a-GFP-ERT2 and H3f3b-RFP-ERT2 but also containing the introns and regulatory regions upstream and downstream the gene sequences (**Figure 3.11B**).

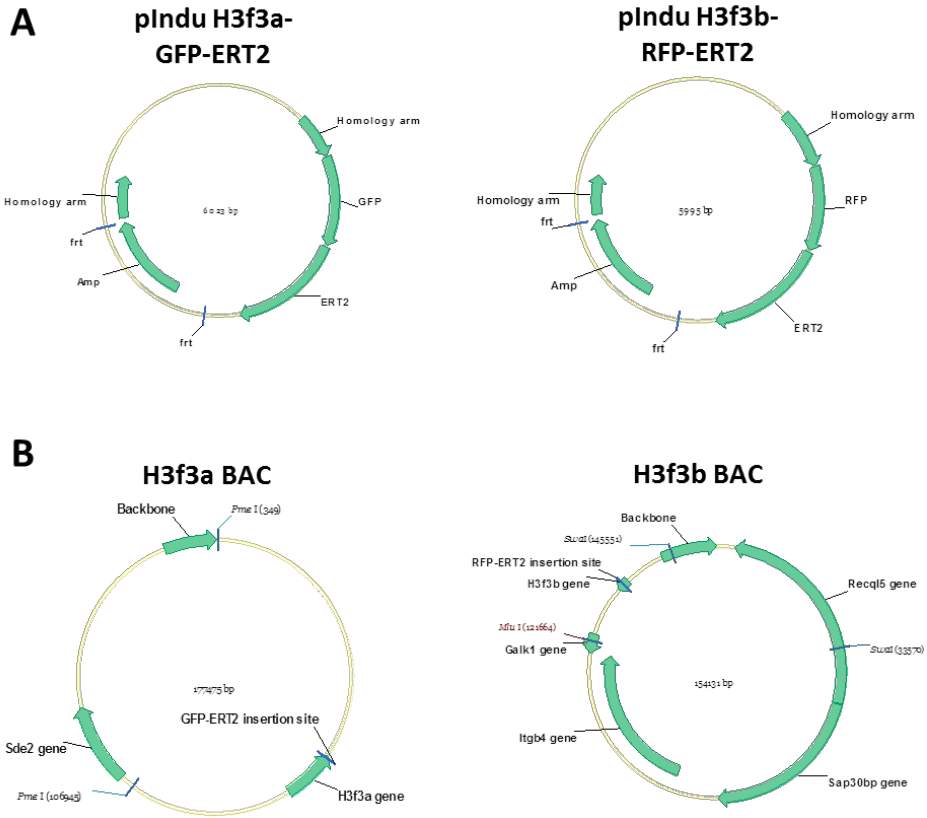

Figure 3.11 pIndu vectors and Bacterial Artificial Chromosomes (BAC) for H3f3a and H3f3b. (A) Maps of the pIndu vectors used to modified the BACs by recombination. **(B)** Maps of each H3f3 BAC showing the backbone region, all genes contained in the BAC and the restriction sites used for the final linearization step.

H3f3a and H3f3b homology arms were amplified by PCR using their respective BACs as templates (**Figure 3.12A**), ERT2 was cut from the pIndu creERT2 vector and GFP and RFP were PCR amplified from RCAS-GFP and RCAS-RFP, respectively (**Figure 3.12B**). Both homology arms plus GFP/RFP and ERT2 were cloned into the pIndu vector using pcDNA 3.1+ as an intermediate vector.

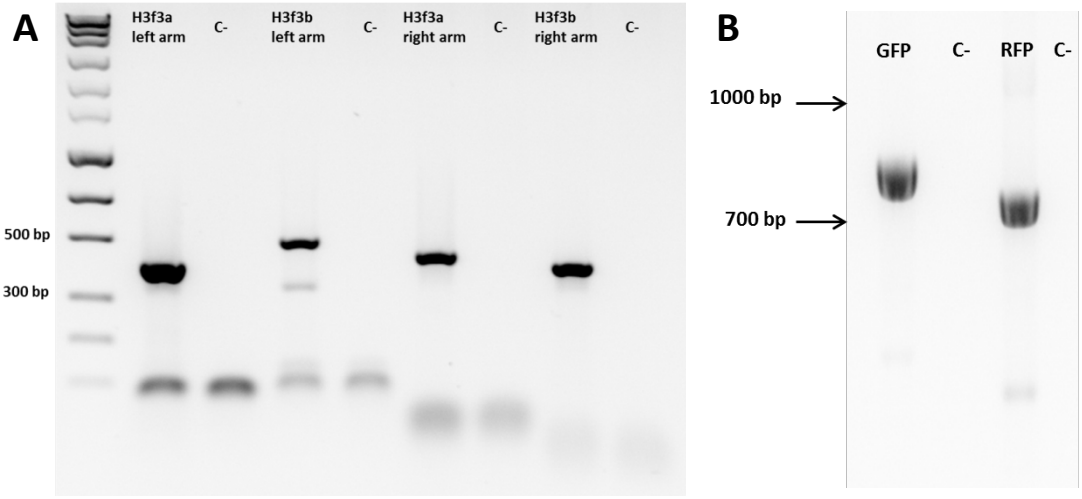

Figure 3.12 PCR amplification of the H3f3 homology arms, GFP and RFP for pIndu cloning. (A) Agarose gel electrophoresis of H3f3 homology arms after PCR amplification. **(B)** Agarose gel electrophoresis of the GFP and RFP inserts after PCR amplification.

4.2.2. H3f3 BACs modification by recombination

Upon reception of the H3f3a and H3f3b BACs, restriction pattern analysis of the BAC DNA was done to confirm the BAC clone identity (**Figure 3.13A** and **B**). H3f3a and H3f3b BACs were modified by homologous recombination using pIndu H3f3a-GFP-ERT2 and pIndu-RFP-ERT2 as described before. After the recombination step, antibiotic resistance was removed from the BAC by activation of the frt sites flanking the ampicillin resistance gene and restriction band pattern analysis confirmed the deletion. Insert region of the BACs (GFP-ERT2/RFP-ERT2) were sequenced confirming the correct recombination and antibiotic resistance removal.

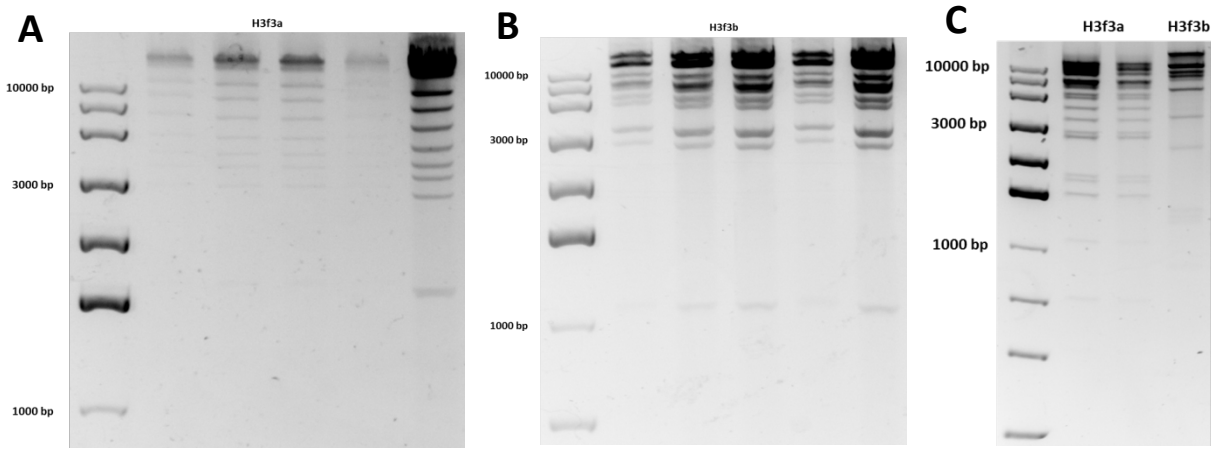

Figure 3.13 BAC restriction fragment pattern analysis on agarose gel. **(A)** Restriction fragment pattern of H3f3a BAC cleaved with ClaI/EcoRV. **(B)** Restriction fragment pattern of H3f3b BAC cleaved with ClaI/EcoRV. **(C)** Restriction fragment pattern of H3f3a-GFP-ERT2 BAC cleaved with AgeI after the antibiotic resistance removal. Restriction fragment pattern of H3f3b-RFP-ERT2 BAC cleaved with NheI after the antibiotic resistance removal.

BAC DNA was linearized and purified prior to microinjection into the zygotes. H3f3a-GFP-ERT2 BAC was linearized using PmeI restriction enzyme, which removed the BAC backbone and the sequence for Sde2 gene also presents while keeping as much upstream and downstream sequence as possible (**Figure 3.11B**). For H3f3b-RFP-ERT2 BAC, the removal of four genes (Recql5, Sap30bp, ltgb4 and Galk1) was necessary to avoid collateral effects from the over-expression of these genes. Owing to that, H3f3b-RFP-ERT2 was linearized using SwaI and MluI sequential digestion which removed the BAC backbone, three of the genes completely and deleted all of the exon sequence from Galk1 gene (**Figure 3.11B**). H3f3b-RFP-ERT2 was purified using a Sepharose column as described before, and fractions containing BAC DNA were identified measuring Absorbance at 260 nm. H3f3b-RFP-ERT2 BAC linearization resulted in the BAC excision into three fragments: one of 25 kb containing our insert of interest that eluted together with a second one of 42 kb, and a third one of 88 kb that eluted later as a second peak in Absorbance. An aliquot of the fractions contained in the first peak of Absorbance were run in a PFGE that confirmed the isolation of the 25 kb fragment in the first fraction (**Figure 3.14A**). H3f3a-GFP-ERT2 BAC linearization resulted in

two fragments: one of 110 kb containing our insert of interest and another one of 70 kb. Sepharose column purification failed to separate both fragments and thus another method was used to purify the insert. After enzymatic restriction of the BAC, the DNA sample was loaded in several contiguous wells and a PFGE was run. After 14 h of PFGE, gel was stopped and wells were excised vertically in two pieces. The first piece containing the marker and one well with sample was post-stained with Ethidium Bromide. The band pattern was used as a guide to excise the 110 kb fragment from the PFGE gel and later post-stained to confirm the correct band excision (**Figure 3.14B**). DNA sample was eluted from the agarose block, concentrated and dialyzed as described before. An aliquot was run in a PFGE to confirm the integrity of the 110 kb fragment, as shown in **Figure 3.14C**.

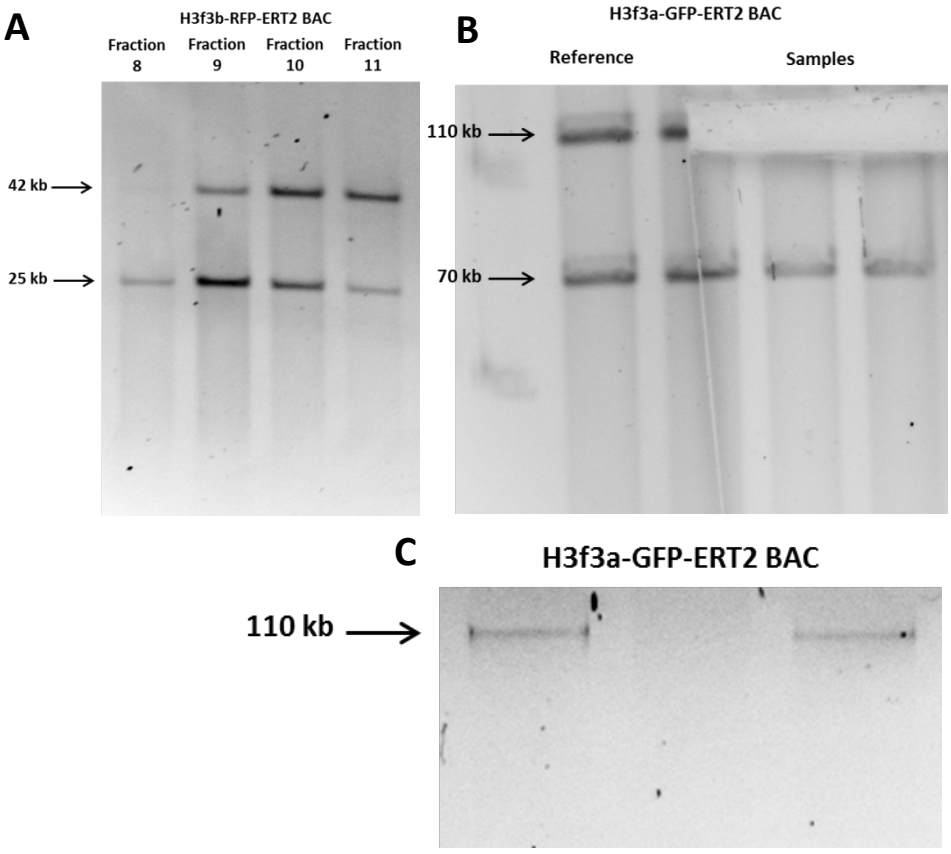

Figure 3.14 BAC purification for DNA microinjection. (A) PFGE of purified fractions from H3f3b-RFP-ERT2 BAC **(B)** PFGE of H3f3a-GFP-ERT2 BAC fragments after PmeI restriction **(C)** PFGE of H3f3a-GFP-ERT2 fragment after dialysis.

The purified DNA samples of H3f3a-GFP-ERT2 and H3f3b-RFP-ERT2 were provided to the Transgenic Service of the DKFZ for DNA microinjection into zygotes.

4.2.3. Identification of chimeras and germ line transmission of H3f3b-RFP-ERT2

Genotyping of the offspring from the females implanted with the microinjected zygotes was performed by PCR analysis to identify chimeras carrying the over-expression constructs (**Figure 3.15A** and **B**). 5 chimeras for H3f3a-GFP-ERT2 were identified and 10 for H3f3b-RFP-ERT2. Chimeras were breed with C57BL/6J wildtype animals to identify founders that achieved germ line transmission. One founder for H3f3b-RFP-ERT2 was identified (Litter B, **Figure 3.15C**) and used to expand the mouse line.

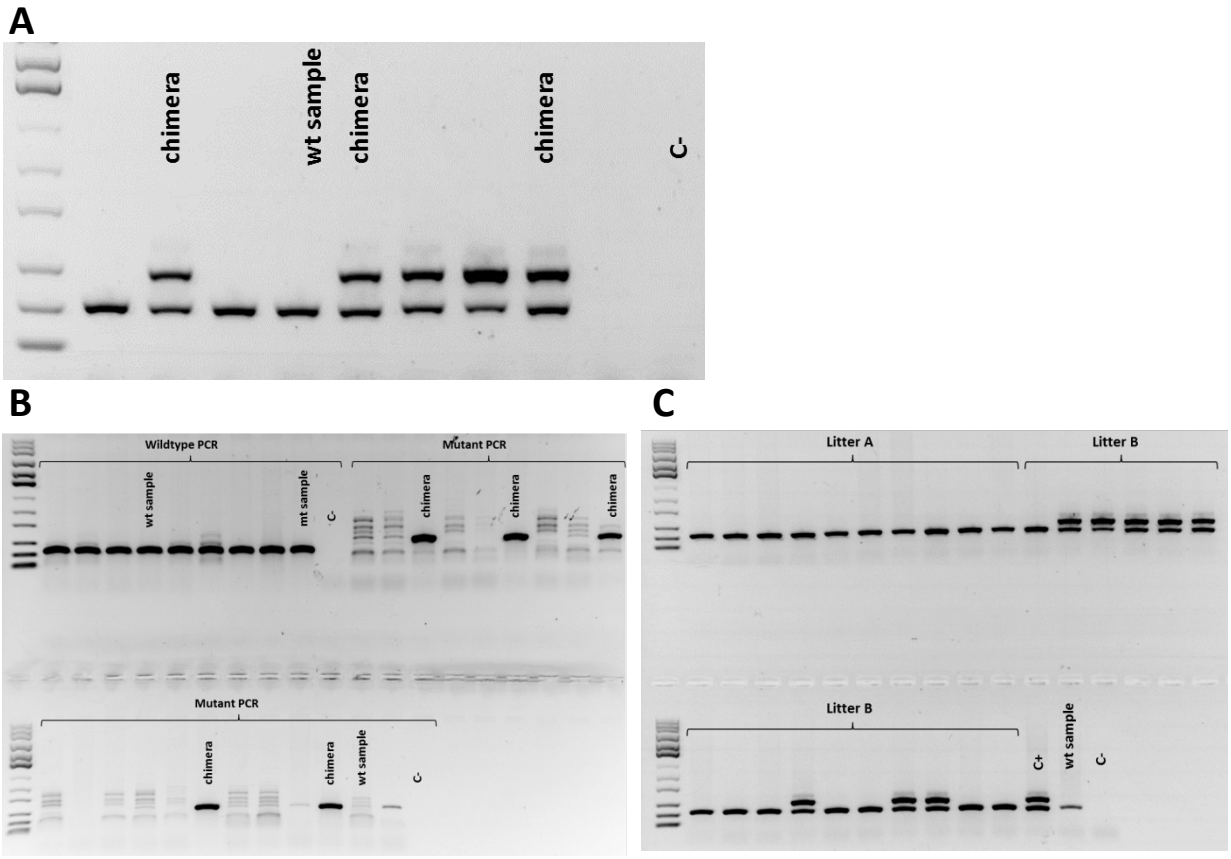

Figure 3.15 Genotyping analysis for identification of founders. (A) Genotyping results for H3f3a-GFP-ERT2 identified 5 potential founders. **(B)** Genotyping results for H3f3b-RFP-ERT2 identified 10 potential founders. **(C)** Genotyping results comparing one litter that achieved germ line transmission (litter B) with one litter that did not achieve it.

5. Discussion

The DIPG field has experienced an outbreak during the last 5 years with several groups adding a significant amount of data to a field that did not see much improvement for the previous 40 years. This input of new data has shed some light about the mechanism of action of the H3.3K27M mutation in these tumors, but has also brought new questions into the field. One of the significant aspects of the field is the lack of a proper model to study DIPG and be able to use it as a platform for treatment studies.

In order to solve this issue, we intended to develop a mouse model for DIPG adapting our established High Grade Glioma model. We designed the H3.3 and H3.3K27M constructs with the following features: we tagged them with GFP to be able to identify the tumor cells carrying our constructs and also with the intention of separating it from the endogenous histone H3.3 in case of further analysis (immunoprecipitation, ChIP-Seq, etc). The sequence cloned into the RCAS vector was floxed to permit us to delete the constructs upon tamoxifen injection. The goal was to develop HGGs carrying the mutant K27M and whenever fully established, delete the mutant histone. By doing this, we would be able to test two main things: first, the role of the K27M mutation in the maintenance of the tumor and second, to assess the feasibility of K27M as a target for therapy. We designed two constructs, one with a mutant H3.3K27M and one with a wildtype H3.3 to be used as a control. Since our model is based on over-expression of H3.3K27M, we consider appropriate to include two different control groups: one without the mutant histone in which over-expression of AKT and PDGFB induced the tumor formation and a second one, consisting of the overexpression of a wildtype H3.3 in combination with AKT and PDGFB to assess de possible impact of having an extra histone H3.3 gene.

We successfully integrated these two constructs in our tumor model which resembled HGG. We could observe pathological features mainly present in GBM like pseudopalysading necrosis, high proliferation and active angiogenesis. Due to the addition of the RCAS-luciferase construct, in vivo tumor growth monitoring was possible by BLI. Our tumor model reproducibly expressed tagged H3.3/H3.3K27M, however a certain degree of penetrance was observed for this trait. A small subset of the tumors displayed what looked like different compartments in which GFP and non-GFP cells have separated spatial locations, but most of the tumors that displayed a significant amount of non-GFP cells within the tumor region showed coexistence of both GFP and non-GFP cells. One possibility to explain this phenomenon would be the fact that our tumor model gives rise to tumors coming from more than one clone. Given the fact that our survival data doesn't show a significant difference between the GFP, H3.3 and K27M group, one could expect that two clones with a different set of mutations might coexist without one overgrowing the other. For example, a H3.3 group tumor could arise from two different clones: clone A over-expressing AKT and PDGFB would show no GFP expression while clone B over-expressing AKT, PDGFB and H3.3-GFP would show GFP expression. Another possible explanation would be that some tumor cells switch-off the expression of the GFP-expressing constructs giving rise to what would look like multi-clonal tumors. To further assess this, genotyping of DNA from a GFP-expressing tumor region versus a non-GFP-expressing tumor region could be done to confirm the presence of the tagged construct DNA in the cells.

In order to better mimic the DIPG in our model, we tried to adjust our tumor induction location from the SVZ to the pons where DIPG are found in patients. We could successfully target the pons in newborn pups but the tumors arising from it using our model did not show HGGs features. The tumor region was mainly restricted to the dorsal pons and the tumor area was small. Hydrocephaly was predominant in the animals with frequent blood clots present in the area between the pons and the cerebellum, usually of considerable size even covering the cerebellum completely. Despite the fact of a reduction in the number of cells injected in the pons (20000 cells per construct versus 40000 cells per construct for the SVZ injection) animals seems to die too early due to the hydrocephaly before the tumors could be fully established. Given the aggressiveness of our tumor model, rapid tumor growth within the pons is the most likely cause of hydrocephaly by blockage of the CSF flow in the ventricles. One possible improvement of the model to be able to adapt to the pons location would be eliminating the injection of the AKT oncogene. Previous data in our lab has shown that PDGFB over-expression alone is able to induce tumors in which animals displayed a significant higher mean survival. A less aggressive tumor approach in the pons may lead to a better histological display as well as the possibility of the K27M mutant making a higher impact in survival than in our current model. A recent study (Mohammad et al., 2017), showed a DIPG mouse model in which mouse NSCs expressing PDGFB and K27M were injected in the pons and developed tumors displaying worse survival than NSCs expressing PDGFB and wildtype H3.3. This data supports the idea that the combination of PDGFB and AKT might be tumorigenic enough such that K27M addition would not make a difference.

Our tumor model for DIPG showed that K27M over-expression significantly reduced H3K27me3 levels in the tumors compared to the control groups. Furthermore, tamoxifen-mediated deletion of K27M rescued the H3K27me3 levels. The increase of H3K27me3 ratio in K27M cre- tumors, when counting total cells, is probably due to the presence of non-tumor cells within the tumor and as mentioned before, because of some tumors presenting a mixture of GFP and non-GFP cells. This also explains the higher standard deviation for this group, accounting for the different ratio of GFP vs non-GFP cells in a particular tumor. Despite all of this, differences were still highly significant between the K27M cre- group and the other groups.

As discussed before, there was no significant survival difference among the groups. K27M group was close to have significant survival difference with the H3.3 group which could more pronounced in the case of a model without AKT over-expression as already discussed. Survival analysis of each group cre- and cre+ subgroups did not show significant differences. That might lead to the possibility that deletion of K27M does not improve the survival of the tumors. However, taking into consideration that AKT and PDGFB over-expression group survival did not differ much from AKT, PDGFB and K27M over-expression group survival is difficult to discard the possibility that K27M deletion did not alter survival because of the aggressiveness of the control group.

In conclusion, we developed a robust tumor model for DIPG which allows the tracing and inducible deletion of the H3.3K27M in a HGG background.

Following a similar pattern like its role in gliomagenesis, the study of H3.3 role in the brain is a rapidly growing field. Over the last years several studies have linked H3.3 with important brain functions such as contextual fear memory but more importantly the discovery of H3.3

accumulation in the brain over age points at a greater involvement of H3.3 in a variety of brain functions. To contribute in this search we planned to establish tools to study H3.3 function in the brain. Histone tracing in living behaving animals was intended to be achieved making use of an inducible tagged histone H3.3 mouse line. H3.3 is encoded by two different genes H3f3a and H3f3b; therefore two mouse lines were designed. BACs were used to over-express H3f3a and H3f3b to ensure that the modified H3.3 genes would be under the normal regulation and promoter influence. BAC clones were modified to tag H3f3a with GFP and ERT2 while H3f3b was tagged with RFP and ERT2. The use of GFP and RFP would allow us to trace the histone activity in the brain and the use of two different fluorochromes allowed the future combination of both mouse lines. The addition of ERT2 will maintain the fusion protein in the cytoplasm until tamoxifen would be injected releasing the tagged histone to go into the nucleus. With these fusion proteins we would achieve an inducible expression of a tagged H3.3. Using these tools, we would be able to monitor H3.3 activity in a inducible way in the brain under different activities and if combined with different cre lines in a specific cell subtype. We successfully modified H3f3a and H3f3b BAC and used them to microinject zygotes. The resulting chimeras for H3f3a-GFP-ERT2 did not achieve germ line transmission but a founder for H3f3b-RFP-ERT2 was identified and used to establish the mouse line. To further continue with this project, H3f3a-GFP-ERT2 injection could be repeated to accomplish germ line transmission. In addition, H3f3b-RFP-ERT2 mouse line will require more validation. Southern Blot to analyze the copy number integration and tamoxifen injection to confirm the translocation into the nucleus would need to be done before conducting more experiments.

In conclusion, we developed a powerful tool to study H3.3 function in the brain. Additionally, the knowledge resulting from the study of H3.3 function in the brain would impact the

knowledge about H3.3 role in gliomagenesis and vice versa bringing together the results derived from the tools developed in both projects.

6. References

Ahmad, K., and Henikoff, S. (2002). The histone variant H3.3 marks active chromatin by replication-independent nucleosome assembly. Mol Cell *9*, 1191-1200.

Akhmanova, A.S., Bindels, P.C., Xu, J., Miedema, K., Kremer, H., and Hennig, W. (1995). Structure and expression of histone H3.3 genes in Drosophila melanogaster and Drosophila hydei. Genome *38*, 586-600.

Banaszynski, L.A., Wen, D., Dewell, S., Whitcomb, S.J., Lin, M., Diaz, N., Elsasser, S.J., Chapgier, A., Goldberg, A.D., Canaani, E.*, et al.* (2013). Hira-dependent histone H3.3 deposition facilitates PRC2 recruitment at developmental loci in ES cells. Cell *155*, 107-120.

Barski, A., Cuddapah, S., Cui, K., Roh, T.Y., Schones, D.E., Wang, Z., Wei, G., Chepelev, I., and Zhao, K. (2007). High-resolution profiling of histone methylations in the human genome. Cell *129*, 823-837.

Bates, P., Rong, L., Varmus, H.E., Young, J.A., and Crittenden, L.B. (1998). Genetic mapping of the cloned subgroup A avian sarcoma and leukosis virus receptor gene to the TVA locus. J Virol *72*, 2505-2508.

Bates, P., Young, J.A., and Varmus, H.E. (1993). A receptor for subgroup A Rous sarcoma virus is related to the low density lipoprotein receptor. Cell *74*, 1043-1051.

Bax, D.A., Mackay, A., Little, S.E., Carvalho, D., Viana-Pereira, M., Tamber, N., Grigoriadis, A.E., Ashworth, A., Reis, R.M., Ellison, D.W.*, et al.* (2010). A distinct spectrum of copy number aberrations in pediatric high-grade gliomas. Clin Cancer Res *16*, 3368-3377.

Behjati, S., Tarpey, P.S., Presneau, N., Scheipl, S., Pillay, N., Van Loo, P., Wedge, D.C., Cooke, S.L., Gundem, G., Davies, H.*, et al.* (2013). Distinct H3F3A and H3F3B driver mutations define chondroblastoma and giant cell tumor of bone. Nat Genet *45*, 1479-1482.

Bender, S., Tang, Y., Lindroth, A.M., Hovestadt, V., Jones, D.T., Kool, M., Zapatka, M., Northcott, P.A., Sturm, D., Wang, W.*, et al.* (2013). Reduced H3K27me3 and DNA hypomethylation are major drivers of gene expression in K27M mutant pediatric high-grade gliomas. Cancer Cell *24*, 660-672.

Borrelli, E., Nestler, E.J., Allis, C.D., and Sassone-Corsi, P. (2008). Decoding the epigenetic language of neuronal plasticity. Neuron *60*, 961-974.

Braunschweig, U., Hogan, G.J., Pagie, L., and van Steensel, B. (2009). Histone H1 binding is inhibited by histone variant H3.3. EMBO J *28*, 3635-3645.

Brown, Z.Z., Muller, M.M., Jain, S.U., Allis, C.D., Lewis, P.W., and Muir, T.W. (2014). Strategy for "detoxification" of a cancer-derived histone mutant based on mapping its interaction with the methyltransferase PRC2. J Am Chem Soc *136*, 13498-13501.

Buczkowicz, P., Hoeman, C., Rakopoulos, P., Pajovic, S., Letourneau, L., Dzamba, M., Morrison, A., Lewis, P., Bouffet, E., Bartels, U*., et al.* (2014). Genomic analysis of diffuse intrinsic pontine gliomas identifies three molecular subgroups and recurrent activating ACVR1 mutations. Nat Genet *46*, 451-456.

Cancer Genome Atlas Research, N. (2008). Comprehensive genomic characterization defines human glioblastoma genes and core pathways. Nature *455*, 1061-1068.

Cao, R., and Zhang, Y. (2004). SUZ12 is required for both the histone methyltransferase activity and the silencing function of the EED-EZH2 complex. Mol Cell *15*, 57-67.

Chan, K.M., Fang, D., Gan, H., Hashizume, R., Yu, C., Schroeder, M., Gupta, N., Mueller, S., James, C.D., Jenkins, R*., et al.* (2013). The histone H3.3K27M mutation in pediatric glioma reprograms H3K27 methylation and gene expression. Genes Dev *27*, 985-990.

Chen, P., Zhao, J., Wang, Y., Wang, M., Long, H., Liang, D., Huang, L., Wen, Z., Li, W., Li, X*., et al.* (2013). H3.3 actively marks enhancers and primes gene transcription via opening higher-ordered chromatin. Genes Dev *27*, 2109-2124.

Commerford, S.L., Carsten, A.L., and Cronkite, E.P. (1982). Histone turnover within nonproliferating cells. Proc Natl Acad Sci U S A *79*, 1163-1165.

Deal, R.B., Henikoff, J.G., and Henikoff, S. (2010). Genome-wide kinetics of nucleosome turnover determined by metabolic labeling of histones. Science *328*, 1161-1164.

Dion, M.F., Kaplan, T., Kim, M., Buratowski, S., Friedman, N., and Rando, O.J. (2007). Dynamics of replication-independent histone turnover in budding yeast. Science *315*, 1405-1408.

Donaldson, S.S., Laningham, F., and Fisher, P.G. (2006). Advances toward an understanding of brainstem gliomas. J Clin Oncol *24*, 1266-1272.

Drane, P., Ouararhni, K., Depaux, A., Shuaib, M., and Hamiche, A. (2010). The death-associated protein DAXX is a novel histone chaperone involved in the replication-independent deposition of H3.3. Genes Dev *24*, 1253-1265.

Elsasser, S.J., Huang, H., Lewis, P.W., Chin, J.W., Allis, C.D., and Patel, D.J. (2012). DAXX envelops a histone H3.3-H4 dimer for H3.3-specific recognition. Nature *491*, 560-565.

Elsasser, S.J., Noh, K.M., Diaz, N., Allis, C.D., and Banaszynski, L.A. (2015). Histone H3.3 is required for endogenous retroviral element silencing in embryonic stem cells. Nature *522*, 240-244.

Ferlay, J., Soerjomataram, I., Dikshit, R., Eser, S., Mathers, C., Rebelo, M., Parkin, D.M., Forman, D., and Bray, F. (2015). Cancer incidence and mortality worldwide: sources, methods and major patterns in GLOBOCAN 2012. Int J Cancer *136*, E359-386.

Fisher, G.H., Orsulic, S., Holland, E., Hively, W.P., Li, Y., Lewis, B.C., Williams, B.O., and Varmus, H.E. (1999). Development of a flexible and specific gene delivery system for production of murine tumor models. Oncogene *18*, 5253-5260.

Frank, D., Doenecke, D., and Albig, W. (2003). Differential expression of human replacement and cell cycle dependent H3 histone genes. Gene *312*, 135-143.

Fritsch, E.F., and Temin, H.M. (1977). Inhibition of viral DNA synthesis in stationary chicken embryo fibroblasts infected with avian retroviruses. J Virol *24*, 461-469.

Funato, K., Major, T., Lewis, P.W., Allis, C.D., and Tabar, V. (2014). Use of human embryonic stem cells to model pediatric gliomas with H3.3K27M histone mutation. Science *346*, 1529-1533.

Garrick, D., Sharpe, J.A., Arkell, R., Dobbie, L., Smith, A.J., Wood, W.G., Higgs, D.R., and Gibbons, R.J. (2006). Loss of Atrx affects trophoblast development and the pattern of X-inactivation in extraembryonic tissues. PLoS Genet *2*, e58.

Goldberg, A.D., Banaszynski, L.A., Noh, K.M., Lewis, P.W., Elsaesser, S.J., Stadler, S., Dewell, S., Law, M., Guo, X., Li, X*., et al.* (2010). Distinct factors control histone variant H3.3 localization at specific genomic regions. Cell *140*, 678-691.

Greer, P.L., and Greenberg, M.E. (2008). From synapse to nucleus: calcium-dependent gene transcription in the control of synapse development and function. Neuron *59*, 846-860.

Grossman, S.A., Ye, X., Piantadosi, S., Desideri, S., Nabors, L.B., Rosenfeld, M., Fisher, J., and Consortium, N.C. (2010). Survival of patients with newly diagnosed glioblastoma treated with radiation and temozolomide in research studies in the United States. Clin Cancer Res *16*, 2443-2449.

Hargrave, D., Bartels, U., and Bouffet, E. (2006). Diffuse brainstem glioma in children: critical review of clinical trials. Lancet Oncol *7*, 241-248.

Hodl, M., and Basler, K. (2009). Transcription in the absence of histone H3.3. Curr Biol *19*, 1221-1226.

Holland, E.C., and Varmus, H.E. (1998). Basic fibroblast growth factor induces cell migration and proliferation after glia-specific gene transfer in mice. Proc Natl Acad Sci U S A *95*, 1218-1223.

Hughes, S.H. (2004). The RCAS vector system. Folia Biol (Praha) *50*, 107-119.

Humphries, E.H., Glover, C., and Reichmann, M.E. (1981). Rous sarcoma virus infection of synchronized cells establishes provirus integration during S-phase DNA synthesis prior to cellular division. Proc Natl Acad Sci U S A *78*, 2601-2605.

Huse, J.T., Holland, E., and DeAngelis, L.M. (2013). Glioblastoma: molecular analysis and clinical implications. Annu Rev Med *64*, 59-70.

Huse, J.T., and Holland, E.C. (2009). Genetically engineered mouse models of brain cancer and the promise of preclinical testing. Brain Pathol *19*, 132-143.

Jin, C., and Felsenfeld, G. (2007). Nucleosome stability mediated by histone variants H3.3 and H2A.Z. Genes Dev *21*, 1519-1529.

Jin, C., Zang, C., Wei, G., Cui, K., Peng, W., Zhao, K., and Felsenfeld, G. (2009). H3.3/H2A.Z double variant-containing nucleosomes mark 'nucleosome-free regions' of active promoters and other regulatory regions. Nat Genet *41*, 941-945.

Jones, C., and Baker, S.J. (2014). Unique genetic and epigenetic mechanisms driving paediatric diffuse high-grade glioma. Nat Rev Cancer *14*.

Kraushaar, D.C., Jin, W., Maunakea, A., Abraham, B., Ha, M., and Zhao, K. (2013). Genome-wide incorporation dynamics reveal distinct categories of turnover for the histone variant H3.3. Genome Biol *14*, R121.

Krimer, D.B., Cheng, G., and Skoultchi, A.I. (1993). Induction of H3.3 replacement histone mRNAs during the precommitment period of murine erythroleukemia cell differentiation. Nucleic Acids Res *21*, 2873-2879.

Lewis, P.W., Elsaesser, S.J., Noh, K.M., Stadler, S.C., and Allis, C.D. (2010). Daxx is an H3.3-specific histone chaperone and cooperates with ATRX in replication-independent chromatin assembly at telomeres. Proc Natl Acad Sci U S A *107*, 14075-14080.

Lewis, P.W., Muller, M.M., Koletsky, M.S., Cordero, F., Lin, S., Banaszynski, L.A., Garcia, B.A., Muir, T.W., Becher, O.J., and Allis, C.D. (2013). Inhibition of PRC2 activity by a gain-of-function H3 mutation found in pediatric glioblastoma. Science *340*, 857-861.

Ligon, K.L., Alberta, J.A., Kho, A.T., Weiss, J., Kwaan, M.R., Nutt, C.L., Louis, D.N., Stiles, C.D., and Rowitch, D.H. (2004). The oligodendroglial lineage marker OLIG2 is universally expressed in diffuse gliomas. J Neuropathol Exp Neurol *63*, 499-509.

Lin, C.J., Conti, M., and Ramalho-Santos, M. (2013). Histone variant H3.3 maintains a decondensed chromatin state essential for mouse preimplantation development. Development *140*, 3624-3634.

Liu, H.K., Belz, T., Bock, D., Takacs, A., Wu, H., Lichter, P., Chai, M., and Schutz, G. (2008). The nuclear receptor tailless is required for neurogenesis in the adult subventricular zone. Genes Dev *22*, 2473-2478.

Liu, H.K., Wang, Y., Belz, T., Bock, D., Takacs, A., Radlwimmer, B., Barbus, S., Reifenberger, G., Lichter, P., and Schutz, G. (2010). The nuclear receptor tailless induces long-term neural stem cell expansion and brain tumor initiation. Genes Dev *24*, 683-695.

Margueron, R., and Reinberg, D. (2011). The Polycomb complex PRC2 and its mark in life. Nature *469*, 343-349.

Maria, B.L., Rehder, K., Eskin, T.A., Hamed, L.M., Fennell, E.B., Quisling, R.G., Mickle, J.P., Marcus, R.B., Jr., Drane, W.E., Mendenhall, N.P*., et al.* (1993). Brainstem glioma: I. Pathology, clinical features, and therapy. J Child Neurol *8*, 112-128.

Marzluff, W.F., Gongidi, P., Woods, K.R., Jin, J., and Maltais, L.J. (2002). The human and mouse replication-dependent histone genes. Genomics *80*, 487-498.

Maze, I., Noh, K.M., and Allis, C.D. (2013). Histone regulation in the CNS: basic principles of epigenetic plasticity. Neuropsychopharmacology *38*, 3-22.

Maze, I., Noh, K.M., Soshnev, A.A., and Allis, C.D. (2014). Every amino acid matters: essential contributions of histone variants to mammalian development and disease. Nat Rev Genet *15*, 259-271.

Maze, I., Wenderski, W., Noh, K.M., Bagot, R.C., Tzavaras, N., Purushothaman, I., Elsasser, S.J., Guo, Y., Ionete, C., Hurd, Y.L*., et al.* (2015). Critical Role of Histone Turnover in Neuronal Transcription and Plasticity. Neuron *87*, 77-94.

McNally, A.G., Poplawski, S.G., Mayweather, B.A., White, K.M., and Abel, T. (2016). Characterization of a Novel Chromatin Sorting Tool Reveals Importance of Histone Variant H3.3 in Contextual Fear Memory and Motor Learning. Front Mol Neurosci *9*, 11.

Michaelson, J.S., Bader, D., Kuo, F., Kozak, C., and Leder, P. (1999). Loss of Daxx, a promiscuously interacting protein, results in extensive apoptosis in early mouse development. Genes Dev *13*, 1918-1923.

Michod, D., Bartesaghi, S., Khelifi, A., Bellodi, C., Berliocchi, L., Nicotera, P., and Salomoni, P. (2012). Calcium-dependent dephosphorylation of the histone chaperone DAXX regulates H3.3 loading and transcription upon neuronal activation. Neuron *74*, 122-135.

Mikkelsen, T.S., Ku, M., Jaffe, D.B., Issac, B., Lieberman, E., Giannoukos, G., Alvarez, P., Brockman, W., Kim, T.K., Koche, R.P.*, et al.* (2007). Genome-wide maps of chromatin state in pluripotent and lineage-committed cells. Nature *448*, 553-560.

Mito, Y., Henikoff, J.G., and Henikoff, S. (2005). Genome-scale profiling of histone H3.3 replacement patterns. Nat Genet *37*, 1090-1097.

Mohammad, F., Weissmann, S., Leblanc, B., Pandey, D.P., Hojfeldt, J.W., Comet, I., Zheng, C., Johansen, J.V., Rapin, N., Porse, B.T.*, et al.* (2017). EZH2 is a potential therapeutic target for H3K27M-mutant pediatric gliomas. Nat Med *23*, 483-492.

Nekrasov, M., Klymenko, T., Fraterman, S., Papp, B., Oktaba, K., Kocher, T., Cohen, A., Stunnenberg, H.G., Wilm, M., and Muller, J. (2007). Pcl-PRC2 is needed to generate high levels of H3-K27 trimethylation at Polycomb target genes. EMBO J *26*, 4078-4088.

Ng, R.K., and Gurdon, J.B. (2008). Epigenetic memory of an active gene state depends on histone H3.3 incorporation into chromatin in the absence of transcription. Nat Cell Biol *10*, 102-109.

Oh, J., Julias, J.G., Ferris, A.L., and Hughes, S.H. (2002). Construction and characterization of a replication-competent retroviral shuttle vector plasmid. J Virol *76*, 1762-1768.

Ohgaki, H., and Kleihues, P. (2007). Genetic pathways to primary and secondary glioblastoma. Am J Pathol *170*, 1445-1453.

Ostrom, Q.T., Bauchet, L., Davis, F.G., Deltour, I., Fisher, J.L., Langer, C.E., Pekmezci, M., Schwartzbaum, J.A., Turner, M.C., Walsh, K.M.*, et al.* (2014). The epidemiology of glioma in adults: a "state of the science" review. Neuro Oncol *16*, 896-913.

Parsons, D.W., Jones, S., Zhang, X., Lin, J.C., Leary, R.J., Angenendt, P., Mankoo, P., Carter, H., Siu, I.M., Gallia, G.L.*, et al.* (2008). An integrated genomic analysis of human glioblastoma multiforme. Science *321*, 1807-1812.

Paugh, B.S., Broniscer, A., Qu, C., Miller, C.P., Zhang, J., Tatevossian, R.G., Olson, J.M., Geyer, J.R., Chi, S.N., da Silva, N.S.*, et al.* (2011). Genome-wide analyses identify recurrent

amplifications of receptor tyrosine kinases and cell-cycle regulatory genes in diffuse intrinsic pontine glioma. J Clin Oncol *29*, 3999-4006.

Paugh, B.S., Qu, C., Jones, C., Liu, Z., Adamowicz-Brice, M., Zhang, J., Bax, D.A., Coyle, B., Barrow, J., Hargrave, D.*, et al.* (2010). Integrated molecular genetic profiling of pediatric high-grade gliomas reveals key differences with the adult disease. J Clin Oncol *28*, 3061-3068.

Peng, J.C., Valouev, A., Swigut, T., Zhang, J., Zhao, Y., Sidow, A., and Wysocka, J. (2009). Jarid2/Jumonji coordinates control of PRC2 enzymatic activity and target gene occupancy in pluripotent cells. Cell *139*, 1290-1302.

Pina, B., and Suau, P. (1987). Changes in histones H2A and H3 variant composition in differentiating and mature rat brain cortical neurons. Dev Biol *123*, 51-58.

Polo, S.E., Roche, D., and Almouzni, G. (2006). New histone incorporation marks sites of UV repair in human cells. Cell *127*, 481-493.

Puget, S., Philippe, C., Bax, D.A., Job, B., Varlet, P., Junier, M.P., Andreiuolo, F., Carvalho, D., Reis, R., Guerrini-Rousseau, L.*, et al.* (2012). Mesenchymal transition and PDGFRA amplification/mutation are key distinct oncogenic events in pediatric diffuse intrinsic pontine gliomas. PLoS One *7*, e30313.

Qu, H.Q., Jacob, K., Fatet, S., Ge, B., Barnett, D., Delattre, O., Faury, D., Montpetit, A., Solomon, L., Hauser, P.*, et al.* (2010). Genome-wide profiling using single-nucleotide polymorphism arrays identifies novel chromosomal imbalances in pediatric glioblastomas. Neuro Oncol *12*, 153-163.

Ray-Gallet, D., Woolfe, A., Vassias, I., Pellentz, C., Lacoste, N., Puri, A., Schultz, D.C., Pchelintsev, N.A., Adams, P.D., Jansen, L.E.*, et al.* (2011). Dynamics of histone H3 deposition in vivo reveal a nucleosome gap-filling mechanism for H3.3 to maintain chromatin integrity. Mol Cell *44*, 928-941.

Ricard, D., Idbaih, A., Ducray, F., Lahutte, M., Hoang-Xuan, K., and Delattre, J.Y. (2012). Primary brain tumours in adults. Lancet *379*, 1984-1996.

Roberts, C., Sutherland, H.F., Farmer, H., Kimber, W., Halford, S., Carey, A., Brickman, J.M., Wynshaw-Boris, A., and Scambler, P.J. (2002). Targeted mutagenesis of the Hira gene results in gastrulation defects and patterning abnormalities of mesoendodermal derivatives prior to early embryonic lethality. Mol Cell Biol *22*, 2318-2328.

Rufiange, A., Jacques, P.E., Bhat, W., Robert, F., and Nourani, A. (2007). Genome-wide replication-independent histone H3 exchange occurs predominantly at promoters and implicates H3 K56 acetylation and Asf1. Mol Cell *27*, 393-405.

Sakai, A., Schwartz, B.E., Goldstein, S., and Ahmad, K. (2009). Transcriptional and developmental functions of the H3.3 histone variant in Drosophila. Curr Biol *19*, 1816-1820.

Sarma, K., Margueron, R., Ivanov, A., Pirrotta, V., and Reinberg, D. (2008). Ezh2 requires PHF1 to efficiently catalyze H3 lysine 27 trimethylation in vivo. Mol Cell Biol *28*, 2718-2731.

Savas, J.N., Toyama, B.H., Xu, T., Yates, J.R., 3rd, and Hetzer, M.W. (2012). Extremely long-lived nuclear pore proteins in the rat brain. Science *335*, 942.

Savla, U., Benes, J., Zhang, J., and Jones, R.S. (2008). Recruitment of Drosophila Polycomb-group proteins by Polycomblike, a component of a novel protein complex in larvae. Development *135*, 813-817.

Schenk, R., Jenke, A., Zilbauer, M., Wirth, S., and Postberg, J. (2011). H3.5 is a novel hominid-specific histone H3 variant that is specifically expressed in the seminiferous tubules of human testes. Chromosoma *120*, 275-285.

Schneiderman, J.I., Orsi, G.A., Hughes, K.T., Loppin, B., and Ahmad, K. (2012). Nucleosome-depleted chromatin gaps recruit assembly factors for the H3.3 histone variant. Proc Natl Acad Sci U S A *109*, 19721-19726.

Schwartzentruber, J., Korshunov, A., Liu, X.Y., Jones, D.T., Pfaff, E., Jacob, K., Sturm, D., Fontebasso, A.M., Quang, D.A., Tonjes, M.*, et al.* (2012). Driver mutations in histone H3.3 and chromatin remodelling genes in paediatric glioblastoma. Nature *482*, 226-231.

Shen, X., Kim, W., Fujiwara, Y., Simon, M.D., Liu, Y., Mysliwiec, M.R., Yuan, G.C., Lee, Y., and Orkin, S.H. (2009). Jumonji modulates polycomb activity and self-renewal versus differentiation of stem cells. Cell *139*, 1303-1314.

Shi, L., Wen, H., and Shi, X. (2016). The Histone Variant H3.3 in Transcriptional Regulation and Human Disease. J Mol Biol.

Shu, H., Nakamura, M., Siretskiy, A., Borghi, L., Moraes, I., Wildhaber, T., Gruissem, W., and Hennig, L. (2014). Arabidopsis replacement histone variant H3.3 occupies promoters of regulated genes. Genome Biol *15*, R62.

Stiller, C.A. (1994). Population based survival rates for childhood cancer in Britain, 1980-91. BMJ *309*, 1612-1616.

Stroud, H., Otero, S., Desvoyes, B., Ramirez-Parra, E., Jacobsen, S.E., and Gutierrez, C. (2012). Genome-wide analysis of histone H3.1 and H3.3 variants in Arabidopsis thaliana. Proc Natl Acad Sci U S A *109*, 5370-5375.

Sturm, D., Bender, S., Jones, D.T., Lichter, P., Grill, J., Becher, O., Hawkins, C., Majewski, J., Jones, C., Costello, J.F.*, et al.* (2014). Paediatric and adult glioblastoma: multiform (epi)genomic culprits emerge. Nat Rev Cancer *14*, 92-107.

Sturm, D., Witt, H., Hovestadt, V., Khuong-Quang, D.A., Jones, D.T., Konermann, C., Pfaff, E., Tonjes, M., Sill, M., Bender, S.*, et al.* (2012). Hotspot mutations in H3F3A and IDH1 define distinct epigenetic and biological subgroups of glioblastoma. Cancer Cell *22*, 425-437.

Sun, H., Damez-Werno, D.M., Scobie, K.N., Shao, N.Y., Dias, C., Rabkin, J., Koo, J.W., Korb, E., Bagot, R.C., Ahn, F.H.*, et al.* (2015). ACF chromatin-remodeling complex mediates stress-induced depressive-like behavior. Nat Med *21*, 1146-1153.

Suto, R.K., Clarkson, M.J., Tremethick, D.J., and Luger, K. (2000). Crystal structure of a nucleosome core particle containing the variant histone H2A.Z. Nat Struct Biol *7*, 1121-1124.

Szenker, E., Lacoste, N., and Almouzni, G. (2012). A developmental requirement for HIRA-dependent H3.3 deposition revealed at gastrulation in Xenopus. Cell Rep *1*, 730-740.

Szenker, E., Ray-Gallet, D., and Almouzni, G. (2011). The double face of the histone variant H3.3. Cell Res *21*, 421-434.

Tamura, T., Smith, M., Kanno, T., Dasenbrock, H., Nishiyama, A., and Ozato, K. (2009). Inducible deposition of the histone variant H3.3 in interferon-stimulated genes. J Biol Chem *284*, 12217-12225.

Tang, M.C., Jacobs, S.A., Mattiske, D.M., Soh, Y.M., Graham, A.N., Tran, A., Lim, S.L., Hudson, D.F., Kalitsis, P., O'Bryan, M.K.*, et al.* (2015). Contribution of the two genes encoding histone variant h3.3 to viability and fertility in mice. PLoS Genet *11*, e1004964.

Thakar, A., Gupta, P., Ishibashi, T., Finn, R., Silva-Moreno, B., Uchiyama, S., Fukui, K., Tomschik, M., Ausio, J., and Zlatanova, J. (2009). H2A.Z and H3.3 histone variants affect nucleosome structure: biochemical and biophysical studies. Biochemistry *48*, 10852-10857.

Torres-Padilla, M.E., Bannister, A.J., Hurd, P.J., Kouzarides, T., and Zernicka-Goetz, M. (2006). Dynamic distribution of the replacement histone variant H3.3 in the mouse oocyte and preimplantation embryos. Int J Dev Biol *50*, 455-461.

Toyama, B.H., Savas, J.N., Park, S.K., Harris, M.S., Ingolia, N.T., Yates, J.R., 3rd, and Hetzer, M.W. (2013). Identification of long-lived proteins reveals exceptional stability of essential cellular structures. Cell *154*, 971-982.

Varmus, H.E., Padgett, T., Heasley, S., Simon, G., and Bishop, J.M. (1977). Cellular functions are required for the synthesis and integration of avian sarcoma virus-specific DNA. Cell *11*, 307-319.

Vogelstein, B., Papadopoulos, N., Velculescu, V.E., Zhou, S., Diaz, L.A., Jr., and Kinzler, K.W. (2013). Cancer genome landscapes. Science *339*, 1546-1558.

von Werder, A., Seidler, B., Schmid, R.M., Schneider, G., and Saur, D. (2012). Production of avian retroviruses and tissue-specific somatic retroviral gene transfer in vivo using the RCAS/TVA system. Nat Protoc *7*, 1167-1183.

Walker, E., Chang, W.Y., Hunkapiller, J., Cagney, G., Garcha, K., Torchia, J., Krogan, N.J., Reiter, J.F., and Stanford, W.L. (2010). Polycomb-like 2 associates with PRC2 and regulates transcriptional networks during mouse embryonic stem cell self-renewal and differentiation. Cell Stem Cell *6*, 153-166.

Wang, S., Robertson, G.P., and Zhu, J. (2004). A novel human homologue of Drosophila polycomblike gene is up-regulated in multiple cancers. Gene *343*, 69-78.

Wang, Y., Yang, J., Zheng, H., Tomasek, G.J., Zhang, P., McKeever, P.E., Lee, E.Y., and Zhu, Y. (2009). Expression of mutant p53 proteins implicates a lineage relationship between neural stem cells and malignant astrocytic glioma in a murine model. Cancer Cell *15*, 514-526.

Wenderski, W., and Maze, I. (2016). Histone turnover and chromatin accessibility: Critical mediators of neurological development, plasticity, and disease. Bioessays *38*, 410-419.

Wiedemann, S.M., Mildner, S.N., Bonisch, C., Israel, L., Maiser, A., Matheisl, S., Straub, T., Merkl, R., Leonhardt, H., Kremmer, E.*, et al.* (2010). Identification and characterization of two novel primate-specific histone H3 variants, H3.X and H3.Y. J Cell Biol *190*, 777-791.

Witt, O., Albig, W., and Doenecke, D. (1996). Testis-specific expression of a novel human H3 histone gene. Exp Cell Res *229*, 301-306.

Wollmann, H., Holec, S., Alden, K., Clarke, N.D., Jacques, P.E., and Berger, F. (2012). Dynamic deposition of histone variant H3.3 accompanies developmental remodeling of the Arabidopsis transcriptome. PLoS Genet *8*, e1002658.

Wu, G., Broniscer, A., McEachron, T.A., Lu, C., Paugh, B.S., Becksfort, J., Qu, C., Ding, L., Huether, R., Parker, M.*, et al.* (2012). Somatic histone H3 alterations in pediatric diffuse intrinsic pontine gliomas and non-brainstem glioblastomas. Nat Genet *44*, 251-253.

Wu, G., Diaz, A.K., Paugh, B.S., Rankin, S.L., Ju, B., Li, Y., Zhu, X., Qu, C., Chen, X., Zhang, J.*, et al.* (2014). The genomic landscape of diffuse intrinsic pontine glioma and pediatric non-brainstem high-grade glioma. Nat Genet *46*, 444-450.

Xiong, C., Wen, Z., and Li, G. (2016). Histone Variant H3.3: A versatile H3 variant in health and in disease. Sci China Life Sci *59*, 245-256.

Zhu, Z., Khan, M.A., Weiler, M., Blaes, J., Jestaedt, L., Geibert, M., Zou, P., Gronych, J., Bernhardt, O., Korshunov, A.*, et al.* (2014). Targeting self-renewal in high-grade brain tumors leads to loss of brain tumor stem cells and prolonged survival. Cell Stem Cell *15*, 185-198.

Zovkic, I.B., Paulukaitis, B.S., Day, J.J., Etikala, D.M., and Sweatt, J.D. (2014). Histone H2A.Z subunit exchange controls consolidation of recent and remote memory. Nature *515*, 582-586.